International Journal of Solids and Structures 271-272 (2023) 112250

Contents lists available at ScienceDirect

International Journal of Solids and Structures

journal homepage: www.elsevier.com/locate/ijsolstr

Impact model of sphere on the coated plate

J. Pan [a,b], Q. Peng [a], X. Liu [a,b,*], Y.G. Wei [c]

[a] LNM, Institute of Mechanics, Chinese Academy of Sciences, Beijing 100190, China
[b] School of Engineering Science, UCAS, Beijing 100049, China
[c] College of Engineering, Peking University, Beijing 100871, China

ARTICLE INFO

Keywords:
Elastic impact
Sphere on coated plate
Soft film
Plate deflection

ABSTRACT

Impacting the coated plate induces flexural waves on the plate, and such dynamic effect can be considered in the Zener model, which couples the vibration of plate with Hertzian contact relationship. However, Zener model is not applicable for deep impact $(\delta_m > \delta_{cr})$ on a coated plate, because the Hertzian contact law requires an assumption that the contact depth cannot be larger than few percent of the film thickness. This assumption renders the Zener model invalid for the deep impact $(\delta_m > \delta_{cr})$ on plate coated with thin film, where high impact velocity may induce deep contact. In this study, we built up a control equation for the deep impact $(\delta_m > \delta_{cr})$ problem of sphere on the plate coated with soft film, where a nonlinear contact relationship different from Hertzian should be used. Then, we obtained an analytical solution by solving the control equation with homotopy analysis method (HAM). Using the analytical solution, we obtained an explicit expression for the contact history of sphere, as well as the vibration history of plate, which enables us to obtain the minimum distance between the impact location and the boundary applicable to the present model and Zener model. What is more, we proposed a model for a critical impact velocity, below which Zener's model applies, and above which the present model does. By comparing with experiments with coated plate in the literature, we found that most experiments should use the present model rather than Zener model.

1. Introduction

Protective coatings are widely used for engineering structures, such as multi-layered armor (Rahimzadeh et al., 2015), polymer coating on vehicle for improved impact resistance of blasting objects, anti-corrosive films (González and Saidman, 2011), as well as anti-wear films preventing abrasion, tearing, and scratches (Lan et al., 2016). In these cases, the metal or glass plate coated with soft film requires the ability to maintain its function after impact loading. Compared to the substrates, these coatings are usually made of softer materials with low elastic modulus such as rubber, polyurea, and plastic.

In the test, the properties of the film can be obtained by analyzing how the soft coating reacts to a contact force. Deep indentation model of soft coating was proposed in a recent study (Argatov et al., 2021), while another study (Liu et al., 2018) proposed a model from nonlinear field theory to describe the large local deformation around the contact area, so that puncture failure of the soft elastomeric membrane can be well predicted. Also, considering large deformation of soft material during contact, study predicted the snap-through instability (excluding plastic instability) of elastomeric membranes when indented by rigid objects (Liu et al., 2022). Considering the coat thickness into effect, Dimitriadis et al. (Dimitriadis et al., 2002) proposed a contact model for deep indentation on coating to illustrate the thickness effect on force–displacement relationship, where the Hertzian contact model may lead to significant errors when applied to thin samples. The robustness of proposed model in this study by Dimitriadis (Dimitriadis et al., 2002) was verified by measuring the elastic modulus of fibroblast cells using Atomic Force Microscopy (Shariyat et al., 2012). Other studies also try to solve the indentation problem on an elastic layer, either theoretically (Argatov, 2011) or numerically (Jaffar, 1988); however, these studies did not give an explicit relationship between contact force and displacement, as Dimitriadis had done in their study (Dimitriadis et al., 2002).

Different from quasi-static indentation, impacting a coated flexible structure exhibits a dynamic effect of two contacted objects. In terms of the vibration of spheres, following the Hertzian impact on an infinite half space by Hunter (Hunter, 1960; Hunter, 1957), Conway studied the dynamic response of a sphere during an elastic impact on a thin film supported by a rigid substrate (Conway et al., 1972; Conway et al., 1970), the obtained impact duration agreed well with the experimental results.

* Corresponding author at: LNM, Institute of Mechanics, Chinese Academy of Sciences, Beijing 100190, China.
E-mail address: xiaomingliu@imech.ac.cn (X. Liu).

https://doi.org/10.1016/j.ijsolstr.2023.112250
Received 14 December 2022; Received in revised form 17 March 2023; Accepted 3 April 2023
Available online 11 April 2023
0020-7683/© 2023 Elsevier Ltd. All rights reserved.

Nomenclature

$\overline{\alpha}_{\max}, \overline{P}, \overline{P}_{\max}, \tau_F, P_0$	Conway's dimensionless maximum contact depth, contact force, maximum contact force and its occurrence time and related parameter, respectively
$2h_1, 2h_2$	Thickness of soft film and thickness of plate, respectively
R	Radius of sphere
F_c	Contact force of Conway's theory
$\delta, \overline{\delta}$	Contact depth and dimensionless contact depth, respectively
E_s, E_1, E_2	Young's modulus of sphere, soft film and plate, respectively
ν_s, ν_1, ν_2	Poisson's ratio of sphere, soft film and plate, respectively
E_s', E_1', E_2'	Equivalent elastic modulus of sphere, soft film and plate, respectively
$F, \overline{F}$	Contact force and dimensionless contact force, respectively
γ	Correction factor of contact force
$t, \overline{t}$	Time and dimensionless time, respectively
m_s	Mass of the sphere
α	Coefficient related to material parameters
ρ_s, ρ_1, ρ_2	Density of sphere, soft film and plate, respectively
D	Bending stiffness of coated plate
V_0	Impact velocity
e	coefficient of restitution
k, k_H	Conway contact stiffness and Hertzian contact stiffness, respectively
T	Time normalization parameter
λ	Dissipation factor
$V' = \sqrt{E_2'/\rho_2}$	Equivalent propagation velocity of longitudinal waves in the plate
$\delta_m, \overline{\delta}_m$	Maximum contact depth and dimensionless maximum contact depth, respectively, obtained from Section 2.3
$V, \overline{V}$	Sphere velocity and dimensionless sphere velocity, respectively
$\overline{\delta}_{0\text{th}}, \overline{\delta}_{1\text{st}}, \overline{\delta}_{n\text{th}}$	The 0th-order, 1st-order solution and nth-order solution of dimensionless maximum contact depth, respectively
β	Exponential term coefficient of the 0th-order solution
ω	Circular frequency of the 0th-order solution
$\overline{\delta}_i, C_{i1}, C_{i2}$	The ith term of the nth-order solution and its two coefficients, respectively
$F_m, \overline{F}_m$	Maximum contact force and dimensionless maximum contact force, respectively
$I, \overline{I}$	Impulse and dimensionless impulse, respectively
$I_t, \overline{I}_t$	Total impulse and dimensionless total impulse, respectively
$t_t, \overline{t}_t$	Total contact duration and dimensionless total contact duration, respectively
$U, \overline{U}$	Deflection of the plate center and its dimensionless expression, respectively
r	Horizontal distance from the coated plate center
$\omega, \overline{\omega}$	Plate deflection history and its dimensionless expression, respectively
$\mathrm{H}(x)$	Function: $\mathrm{H}(x) = \pi/2 - \mathrm{Si}(x) + x\mathrm{Ci}(x) - \sin(x)$
$\mathrm{Si}(x), \mathrm{Ci}(x)$	Sine integral and cosine integral, respectively
$V_F, \overline{V}_F$	Final velocity and dimensionless final velocity of sphere, respectively
W	Kinetic energy loss of sphere
ξ	Ratio of energy loss of sphere
δ_{cr}	Critical depth for the conversion of deep impact ($\delta_m > \delta_{cr}$) and shallow impact ($\delta_m \le \delta_{cr}$), obtained from Section 3.5
V_{cr}	Critical velocity for the conversion of deep impact ($\delta_m > \delta_{cr}$) and shallow impact ($\delta_m \le \delta_{cr}$)
y_0, φ, μ	Coefficients related to material parameters
$\overline{t}_c, \overline{t}_r, \eta$	Dimensionless compression duration, dimensionless recovery duration and asymmetry parameter, respectively
	Variables with asterisk (*) mean that they are the results of the shallow impact ($\delta_m \le \delta_{cr}$) model

Comparisons with the Hertzian impact are shown in the following table.

	Hertz's model	Conway's model
Maximum contact depth	$\overline{\alpha}_{\max} = 1.0934 P_0^{-2}$	$\overline{\alpha}_{\max} = 0.860 P_0^{-5/3}$
Maximum contact force	$\overline{P}_{\max} = \overline{\alpha}_{\max}^{3/2}$	$\overline{P}_{\max} = \frac{3\pi}{4}\overline{\alpha}_{\max}^2$
Time of $\overline{P}_{\max}$	$\tau_F = 1.607 P_0^{-2}$	$\tau_F = 1.206 P_0^{-2}$

In addition, Conway pointed out that, as the lay thickness decreases, the force–displacement switches from $\overline{P} = \overline{\alpha}^{3/2}$ to $\overline{P} = (3\pi/4)\overline{\alpha}^2$. In these studies (Conway et al., 1972; Conway et al., 1970), Conway used a Taylor expansion to fit the switch of power from 1.5 to 2, and numerically solved the control equation of sphere with nonlinear contact law. Based on their experiment, they pointed out that the vibration effects by plate flexural modes might be important, but did not study this issue. Instead, they glued the thin film to a very thick plate to eliminate the vibration effect such that a support by infinite half space can be used.

While for a thin plate under impact, the vibration effect of the plate can be distinguishable. The wave effect on the impact between sphere and thin plate has been studied by Zener (Zener, 1941), who assumed that flexural waves occur after the elastic impact. During the impact with thick plates, two types of flexural waves (longitudinal and shear waves) considering thickness effect are found by both experimental and theoretical investigation (Koller and Kolsky, 1987). By modifying the model and developing further experimental techniques, a comprehensive model (Boettcher et al., 2017b) is able to describe the experimental data better than model of Koller. Boettcher not only considers the influence of the flexural wave, but also discusses the viscous and plastic effect. In addition, for thick plate, this group (Boettcher et al., 2017b) modified the model of Hunter (Hunter, 1957), using Reed's approximation for force–time relation (Reed, 1985), to obtain results with higher accuracy (Boettcher et al., 2017a). In another study (Müller et al., 2016), authors have shown that the contact time during impact is highly related with the vibration of the plate, and this study used a free-fall apparatus to measure the contact time of a low-velocity impact of steel spheres on large thin glass plates; the measured time had been compared with the theoretical predictions of Zener model. Result shows that Zener's model, with wave effect taken into account, can predict the contact behavior during the impact (Müller et al., 2016). The dynamic characteristics of sphere and film, such as Nasrollahi and Rizzo (Nasrollahi and Rizzo, 2020), is used to measure intraocular pressure, however, the dynamic relations are not clear.

For plates coated with soft film, the impact dynamics remains unknown. In this study, we focus on developing an impact model for such coated plate. Researchers (Russell, 2020; Stergiou et al., 2021; Xia et al., 2023) have studied the impact problem of plate with soft coating through experiment and numerical simulation. However, to authors' knowledge, there is no theoretical model in literature to consider the depth-separable contact relationship and the flexural wave of a coated plate during impact. The reasons have two folds. First of all, modeling of shallow and deep indentions on the coated plate requires separate contact laws, as suggested by Conway (Conway et al., 1972; Conway et al., 1970), with power index in the force–displacement relationship switching from 1.5 to 2. Second, there is no universal map to show how

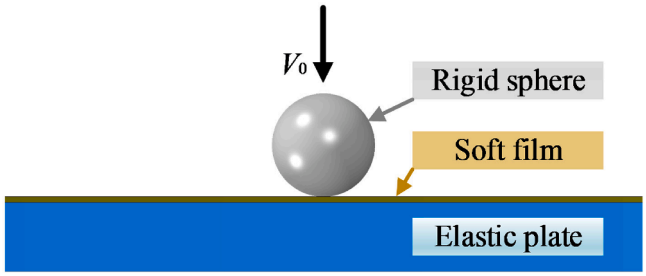

Fig. 1. Schematic diagram of impact model of rigid sphere on plate with soft film.

the dynamic behavior of plate is related to the impact velocity. The different impact velocity may induce different types of contact force law, and thus trigger different levels of flexural waves on the plate.

In this paper, we built a universal law, unveiling the transition from Zener's to Conway's impact considering energy dissipation by flexural waves. The purpose of this paper is to present a comprehensive model for the elastic impact between a sphere and a plate coated with soft material as shown in Fig. 1.

2. Methodology

2.1. Indentation of a coated plate

In this section, we studied the force–displacement relationship of a rigid sphere against a coated plate. The soft film of thickness $2h_1$ is bonded to the plate of thickness $2h_2$, and the radius of the rigid sphere is R. When the indentation depth is shallow, the stress field of film follows the Hertz assumption. On the other hand, when the indentation depth is deep, the Hertz relationship will be violated. By using the stress field of deep indentation of thin film, Conway et al. (Conway et al., 1970) provided the relationship between contact force and depth for deep indentation:

$$F_c = \frac{\pi E_1' R}{2h_1}\delta^2 \tag{1}$$

where δ is the contact depth, $E_i' = E_i/(1-\nu_i^2)$ is the equivalent elastic modulus, E_i is the elastic modulus, ν_i is the Poisson's ratio, and the subscript i is s, 1 and 2, representing the sphere, soft film and plate, respectively.

For a flexible coated plate, due to the bonding constraint of interfaces and the deformation of the plate, Eq. (1) must be modified. As in Appendixes A1 and A2, we parametrically conducted a wide-range of finite element method (FEM) simulations covering various cases, showing that Eq. (1) can be improved by single correction factor γ:

$$F = \frac{\gamma\pi E_1' R}{2h_1}\delta^2 \tag{2}$$

F is the contact force, γ is the correction factor:

$$\gamma = \gamma_1\gamma_2 \tag{3}$$

$$\gamma_1 = G_1 + G_2\left(\frac{E_2}{E_1}\right)^{G_5} + G_3\left(\frac{R}{2h_1}\right)^{G_6} + G_4\left(\frac{E_2}{E_1}\right)^{G_5}\left(\frac{R}{2h_1}\right)^{G_6}$$

$$\gamma_2 = \frac{g_1 + g_2\nu_1 + g_3\nu_2 + g_4\nu_2^2 + g_5\nu_2^3}{1 + g_6\nu_1 + g_7\nu_1^2 + g_8\nu_1^3 + g_9\nu_2 + g_{10}\nu_2^2}$$

where, $G_i(i = 1, 2...6)$ and $\gamma_i(i = 1, 2...10)$ are constants:

$$G_1 = 5.9798 \quad G_2 = -283.54876 \quad G_3 = -4.60697$$
$$G_4 = 283.17337 \quad G_5 = -0.41051 \quad G_6 = -0.00146$$

$$g_1 = 0.95458 \quad g_2 = -0.86196 \quad g_3 = 0.04125 \quad g_4 = 0.13038 \quad g_5 = 0.03515$$
$$g_6 = -1.00497 \quad g_7 = 0.02758 \quad g_8 = -2.13816 \quad g_9 = 0.06728 \quad g_{10} = 0.02767$$

Details are provided in Appendixes A2. In most of the situations, the

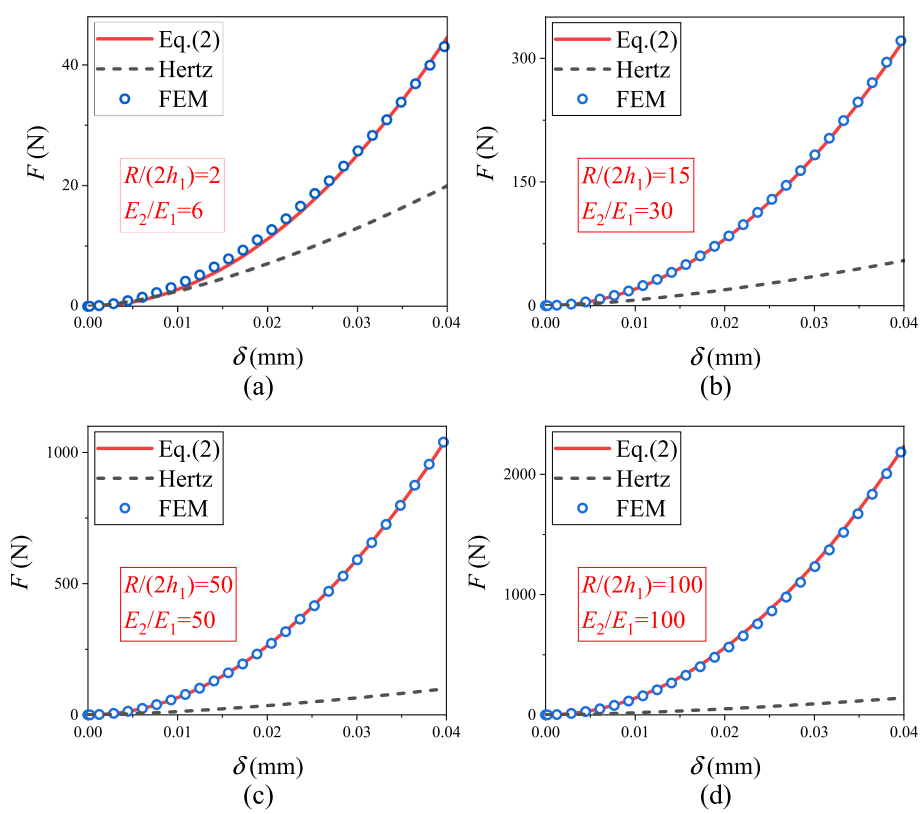

Fig. 2. Comparison of Eq. (2) with FEM results when $R/(2h_1)$ and E_2/E_1 take different values: (a) $R/(2h_1) = 2$, $E_2/E_1 = 6$; (b) $R/(2h_1) = 15$, $E_2/E_1 = 30$; (c) $R/(2h_1) = 50$, $E_2/E_1 = 6 = 50$; (d) $R/(2h_1) = 100$, $E_2/E_1 = 100$.

conditions of $R/2h_1 \geqslant 2$ and $E_2/E_1 \geqslant 6$ apply, and Eq. (2) can well predict the contact behavior, as shown in Fig. 2, while Hertz model underestimates the contact force.

2.2. Impact model of a rigid sphere on a coated plate

For a sphere impacting on a plate, under the assumption that the flexural wave has not been reflected back from the boundary during impact, Zener (Zener, 1941) concluded the control equation as follows.

$$\frac{d^2\delta}{dt^2} + \alpha\frac{dF(\delta)}{dt} + m_s^{-1}F(\delta) = 0 \tag{4}$$

where, t is time, m_s is the mass of sphere, and α is the coefficient related to material parameters and plate thickness. In the case of a coated plate as in Fig. 1, α can be expressed by:

$$\alpha = \frac{1}{8}(2\rho_1 h_1 + 2\rho_2 h_2)^{-1}\left(\frac{2\rho_1 h_1 + 2\rho_2 h_2}{D}\right)^{1/2} \tag{5}$$

where, ρ_1 and ρ_2 are the density of soft film and plate, respectively, and D is the bending stiffness.

Given that the bending stiffness of the coating are negligible with respect to that of the substrate, we assume that the neutral plane of the coated plate is coincident with the mid plane of the substrate. Considering $h_1 << h_2$, and neglecting the higher power term of h_1, we obtain the expression for bending stiffness by integration:

$$D = \frac{2}{3}h_2^3 E_2'\left(1 + \frac{3h_1 E_1'}{h_2 E_2'}\right) \tag{6}$$

Verification with exact value shows that the relative error of Eq. (6) is less than 2.6%. Substitute Eq. (6) into Eq. (5), we obtain:

$$\alpha = \frac{(3\rho_2/E_2')^{1/2}}{16\rho_2 h_2^2}\left(1 + \frac{3h_1 E_1'}{h_2 E_2'}\right)^{-1/2}\left(1 + \frac{\rho_1 h_1}{\rho_2 h_2}\right)^{-1/2} \tag{7}$$

With initial conditions:

$$\begin{cases} \delta|_{t=0} = 0 \\ \left.\frac{d\delta}{dt}\right|_{t=0} = V_0 \end{cases} \tag{8}$$

where V_0 is the impact velocity. The whole impact process can be divided into two distinct stages: a compression stage where contact depth δ increases from 0 to a maximum, and a restitution stage where the sphere recovers its velocity by coefficient of restitution e strictly less than 1:

$$eV_0 = \left.\frac{d\delta}{dt}\right|_{\delta=0, t\neq 0} \tag{9}$$

To model the impact, we use separate expressions for the contact force for shallow impact ($\delta_m \leq \delta_{cr}$) and deep impact ($\delta_m > \delta_{cr}$):

- Under shallow impact ($\delta_m \leq \delta_{cr}$) with low impact velocity, using Hertzian relationship, the control equation writes:

$$\frac{d^2\delta}{dt^2} + \alpha k_H \frac{d}{dt}\left(\delta^{3/2}\right) + m_s^{-1}k_H\delta^{3/2} = 0 \tag{10}$$

where, $k_H = 4E_1' R^{1/2}/3$ is the Hertzian contact stiffness.

- Under deep impact ($\delta_m > \delta_{cr}$) with high impact velocity, using Conway's relationship, substituting Eq. (2) into Eq. (4) yields:

$$\frac{d^2\delta}{dt^2} + \alpha k \frac{d}{dt}\left(\delta^2\right) + m_s^{-1}k\delta^2 = 0 \tag{11}$$

where, $k = \gamma\pi E_1' R/(2h_1)$ is the stiffness of the present corrected relationship of contact.

With boundary and initial conditions, Eqs. (10) and (11) form a complete description for the impact of a sphere on a coated plate. For Eq. (10), our previous study (Peng et al., 2021b) provided an analytical solution, as listed in Section 3.4.

To solve Eq. (11), we non-dimensionalize Eq. (11) by change of variables as follows:

$$\delta = TV_0\bar{\delta} \tag{12}$$

$$t = T\bar{t} \tag{13}$$

with

$$T = \left(\frac{m_s}{kV_0}\right)^{1/3} \tag{14}$$

where $\bar{\delta}$ is the dimensionless contact depth and $\bar{t}$ is the dimensionless time. Eq. (10) can be rewritten as:

$$\frac{d^2\bar{\delta}}{d\bar{t}^2} + 2\lambda\bar{\delta}\frac{d\bar{\delta}}{d\bar{t}} + \bar{\delta}^2 = 0 \tag{15}$$

with initial conditions:

$$\begin{cases} \bar{\delta}|_{\bar{t}=0} = 0 \\ \left.\frac{d\bar{\delta}}{d\bar{t}}\right|_{\bar{t}=0} = 1 \end{cases} \tag{16}$$

Where

$$\lambda = \frac{\alpha m_s}{T} \tag{17}$$

is a parameter relating to the energy dissipation. Under such non-dimensionlization, the coefficient of restitution can be calculated by

$$e = \left.\frac{d\bar{\delta}}{d\bar{t}}\right|_{\bar{\delta}=0, \bar{t}\neq 0} \tag{18}$$

Substituting Eq. (7) in to Eq. (17), we obtain the expression for the dissipation factor λ:

$$\lambda = \frac{\pi}{8\cdot 3^{1/6}}\gamma^{\frac{1}{3}}\left(\frac{V_0}{V'}\right)^{\frac{1}{3}}\left(\frac{\rho_s}{\rho_2}\right)^{\frac{2}{3}}\left(\frac{E_1'}{E_2'}\right)^{\frac{1}{3}}\left(\frac{R}{h_2}\right)^2\left(\frac{R}{h_1}\right)^{\frac{1}{3}}\left(1 + \frac{3h_1 E_1'}{h_2 E_2'}\right)^{-\frac{1}{2}}\left(1 + \frac{\rho_1 h_1}{\rho_2 h_2}\right)^{-\frac{1}{2}} \tag{19}$$

where, $V' = \sqrt{E_2'/\rho_2}$ is the equivalent propagation velocity of longitudinal waves in the plate, ρ_s is the density of sphere. It is shown that with the increase of plate density, thickness and Young's modulus, the dissipation factor λ decreases, suggesting less dissipation by the flexural wave.

2.3. Determine the maximum impact depth

In this section, we develop an approximated expression for the maximal contact depth. Substituting dimensionless velocity $\bar{V} = d\bar{\delta}/d\bar{t}$ into Eq. (15), we obtain:

$$\bar{V}\frac{d\bar{V}}{d\bar{\delta}} + 2\lambda\bar{\delta}\bar{V} + \bar{\delta}^2 = 0 \tag{20}$$

Because Eq. (20) cannot be solved directly. We adopt an approximation as follows. On the one hand, as $\lambda \to \infty$, Eq. (20) becomes $d\bar{V}/d\bar{\delta} + 2\lambda\bar{\delta} = 0$, and the solution is $\bar{V} = 1 - \lambda\bar{\delta}^2$. $\bar{\delta}$ reaches the maximum $\bar{\delta}_m$ when $\bar{V} = 0$. Therefore, we have

$$\bar{\delta}_m^{-2} = \lambda \tag{21}$$

On the other hand, as $\lambda \to 0$, Eq. (20) becomes $\bar{V}(d\bar{V}/d\bar{\delta}) + \bar{\delta}^2 = 0$, the

solution to which is $\overline{V} = \sqrt{1 - 2\overline{\delta}^3/3}$. Therefore, we have:

$$\overline{\delta}_m^{-2} = \left(\frac{3}{2}\right)^{-2/3} \tag{22}$$

Joining Eqs. (21) and (22), we approximate $\overline{\delta}_m$ by $\overline{\delta}_m^{-2} = \lambda + (3/2)^{-2/3}$ and hence:

$$\overline{\delta}_m = \left(\lambda + \left(\frac{3}{2}\right)^{-2/3}\right)^{-1/2} \tag{23}$$

Validation of Eq. (23) with numerical result is shown in Fig. 3(a), and the result shows good agreement, with the relative error less than 1%, as shown in Fig. 3(b).

2.4. Solution to nonlinear differential Eq. (15)

Using the HAM, we can obtain the complete solution to any order. The detailed solution procedures are provided in Appendix A3, where we also show the advantage of HAM to the present problem against method of series expansion. Here, we only list the main results, as follows.

The 0th-order solution is:

$$\overline{\delta}_{0\text{th}} = \overline{\delta}_0 = \frac{1}{\omega} e^{-\beta\overline{t}} \sin(\omega\overline{t}) \tag{24}$$

$$\beta = \frac{(\lambda - 0.125)\overline{\delta}_m}{2} \tag{25}$$

$$\omega = \frac{\sqrt{3.2\overline{\delta}_m - (\lambda - 0.125)^2\overline{\delta}_m^2}}{2} \tag{26}$$

The nth-order solution ($n \geqslant 1$) is:

$$\overline{\delta}_{n\text{th}} = \sum_{i=0}^{n} \overline{\delta}_i \tag{27}$$

where

$$\overline{\delta}_i = e^{-\beta\overline{t}}[C_{i1}(\overline{t})\sin(\omega\overline{t}) + C_{i2}(\overline{t})\cos(\omega\overline{t})] \tag{28}$$

$$\begin{cases} C_{i1}(\overline{t}) = \displaystyle\int_0^{\overline{t}} \frac{\cos(\omega\overline{t})}{\omega} e^{\beta\overline{t}} f_i(\overline{t}) d\overline{t} \\ C_{i2}(\overline{t}) = \displaystyle\int_0^{\overline{t}} -\frac{\sin(\omega\overline{t})}{\omega} e^{\beta\overline{t}} f_i(\overline{t}) d\overline{t} \end{cases} \tag{29}$$

and

$$f_i(\overline{t}) = (\lambda - 0.125)\overline{\delta}_m\dot{\overline{\delta}}_{i-1} + 0.8\overline{\delta}_m\overline{\delta}_{i-1} - 2\lambda\sum_{k=0}^{i-1}\overline{\delta}_k\dot{\overline{\delta}}_{i-1-k} - \sum_{k=0}^{i-1}\overline{\delta}_k\overline{\delta}_{i-1-k} \tag{30}$$

The expression of the 1st-order solution is given by:

$$\overline{\delta}_{1\text{st}} = e^{-\beta\overline{t}}\left\{\begin{array}{l} \sin(\omega\overline{t})\left[\begin{array}{l} \dfrac{1}{\omega} + \dfrac{(\lambda - 0.125)\overline{\delta}_m(0.5\overline{t} + \chi_2)}{\omega} + \dfrac{e^{-\beta\overline{t}}\chi_3}{\omega^3\chi_1} \\ + \dfrac{0.8\overline{\delta}_m\chi_5}{2\omega^3} - \dfrac{(\lambda - 0.125)\beta\overline{\delta}_m\chi_5}{2\omega^3} - \dfrac{2\lambda\beta e^{-\beta\overline{t}}\chi_3}{\chi_1\omega^3} \\ + \dfrac{2\lambda e^{-\beta\overline{t}}}{\omega^2\chi_1}\left(\begin{array}{l} -3\omega^3 e^{\beta\overline{t}} - \omega\beta^2 e^{\beta\overline{t}} - 2\omega\beta^2\cos(\omega\overline{t}) + 2\omega^2\beta\sin(\omega\overline{t}) \\ +3\omega^3\chi_6 + 3\omega\beta^2\chi_6 + \beta^3\chi_7\sin(\omega\overline{t}) + \omega^2\beta\chi_7\sin(\omega\overline{t}) \end{array}\right) \end{array}\right] \\ -\cos(\omega\overline{t})\left[\begin{array}{c} \dfrac{\chi_4}{\omega^3} + \dfrac{0.8\overline{\delta}_m(0.5\overline{t} - \chi_2)}{\omega^2} - \dfrac{2\lambda\beta\chi_4}{\omega^3} \\ + \dfrac{(\lambda - 0.125)\overline{\delta}_m\chi_5}{2\omega^2} - \dfrac{(\lambda - 0.125)\beta\overline{\delta}_m(0.5\overline{t} - \chi_2)}{\omega^2} + \dfrac{2\lambda e^{-\beta\overline{t}}\chi_3}{\omega^2\chi_1} \end{array}\right] \end{array}\right\} \tag{31}$$

where:

Where

$$\begin{aligned} \chi_1 &= \beta^4 + 10\omega^2\beta^2 + 9\omega^4 \\ \chi_2 &= \frac{\sin(2\omega\overline{t})}{4\omega} \\ \chi_3 &= 2\omega^2\beta\chi_6 - 2\omega^2\beta e^{\beta\overline{t}} - 3\omega^3\chi_8 - \beta^2\omega\chi_8 + \beta^3\cos(\omega\overline{t})\chi_5 + 3\beta\omega^2\cos(\omega\overline{t})\chi_5 + 2\beta^2\omega\chi_7\sin(\omega\overline{t}) \\ \chi_4 &= \frac{3\omega}{4\chi_9} - \frac{3\omega}{4\chi_{10}} + \frac{e^{-\beta\overline{t}}}{4}\left[\frac{3\beta\sin(\omega\overline{t}) + 3\omega\cos(\omega\overline{t})}{\chi_{10}} - \frac{\beta\sin(3\omega\overline{t}) + 3\omega\cos(3\omega\overline{t})}{\chi_9}\right] \\ \chi_5 &= \sin^2(\omega\overline{t}) \\ \chi_6 &= \cos^3(\omega\overline{t}) \\ \chi_7 &= \cos^2(\omega\overline{t}) \\ \chi_8 &= \sin^3(\omega\overline{t}) \\ \chi_9 &= \beta^2 + 9\omega^2 \\ \chi_{10} &= \beta^2 + \omega^2 \end{aligned} \tag{32}$$

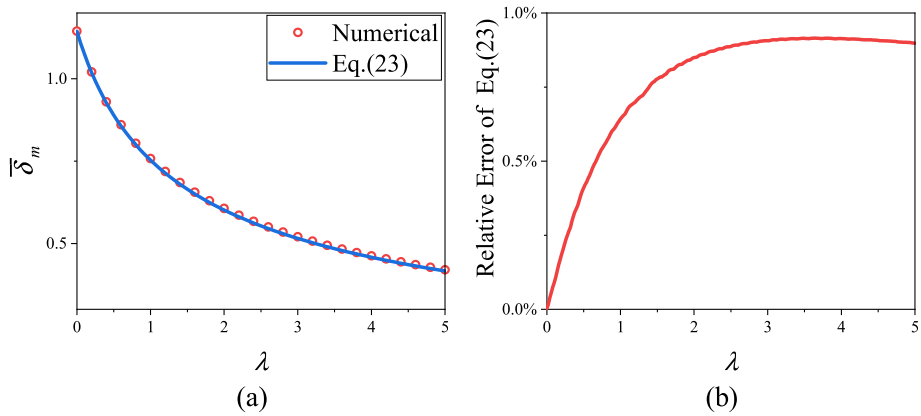

Fig. 3. (a) Comparison between Eq. (23) and Numerical Solution; (b) Relative error of Eq. (23).

3. Result and discussion

Using the results in Section 2, we can investigate various variables such as contact force, contact duration, and coefficient of restitution. In this section, we first compare the present analytical solution with numerical solution (are done by 4-order Runge-Kutta method) and FEM results(model details are in Appendix A1), in terms of dynamic contact depth history, contact force history, sphere velocity history and coated plate deflection history. Then, we study the influence of dissipation factor λ on maximum contact force, contact time, total impulse, ratio of energy loss of sphere and coefficient of restitution.

3.1. History of dynamic contact depth

Fig. 4 plots the present 0th-order, 1st-order, and 2nd-order solutions with the numerical and FEM results. It is evident that the 0th-order, 1st-order, 2nd-order solutions can well depict the depth history. With the increase of the order, the analytical solution quickly converges to the exact numerical solution. Compared with the numerical solution, the relative error of the maximum contact depth is less than 3.9% for the 0th-order solution, 3.3% for the 1st-order solution, and 0.9% for the 2nd-order solution, with λ ranges from 0 to 1.3, as shown in Fig. 5. Because the dissipation factor reflects the intrinsic inelasticity (Note that the dissipation of external energy by elastic waves, not involving plasticity or viscosity) of the plate (Zener, 1941), with the increase of dissipation factor λ, the asymmetry of contact depth history increases, the maximum contact depth decreases and the contact recovery time increases.

With Eq.(2), we obtain an expression for the contact force, proportional to the contact depth to the power of 2:

$$F = k\delta^2 = k(TV_0\overline{\delta})^2 = k^{\frac{1}{3}}m_s^{\frac{2}{3}}V_0^{\frac{4}{3}}\overline{\delta}^2 \tag{33}$$

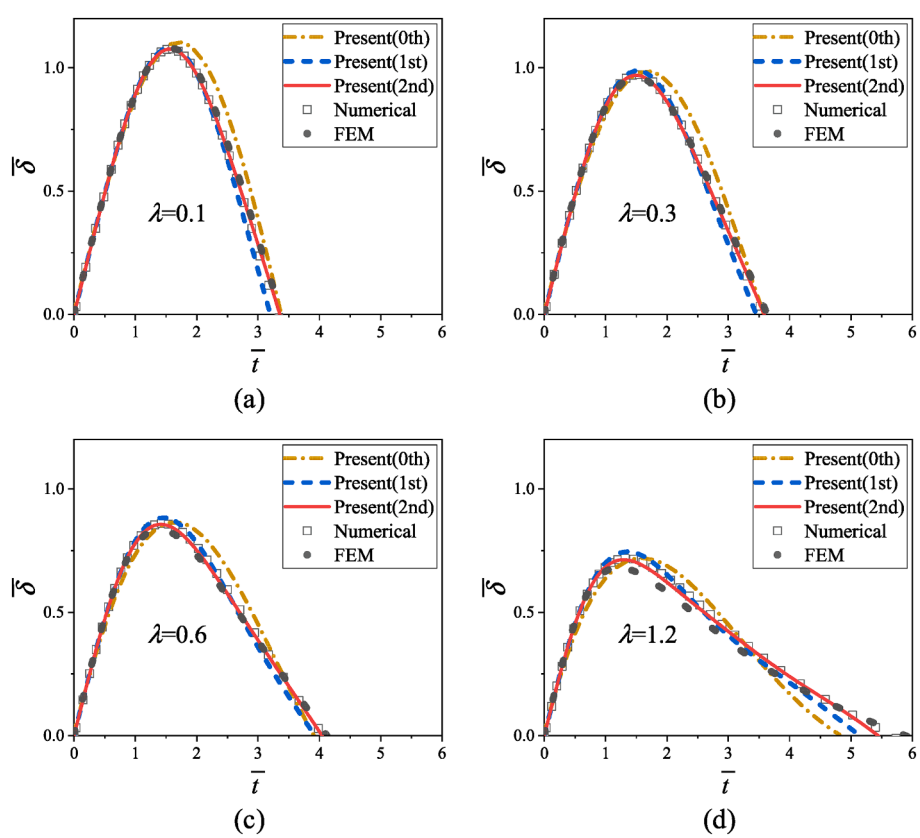

Fig. 4. Comparisons of analytical, numerical and FEM results for contact depth-time: (a) $\lambda = 0.1$; (b) $\lambda = 0.3$; (c) $\lambda = 0.6$; (d) $\lambda = 1.2$.

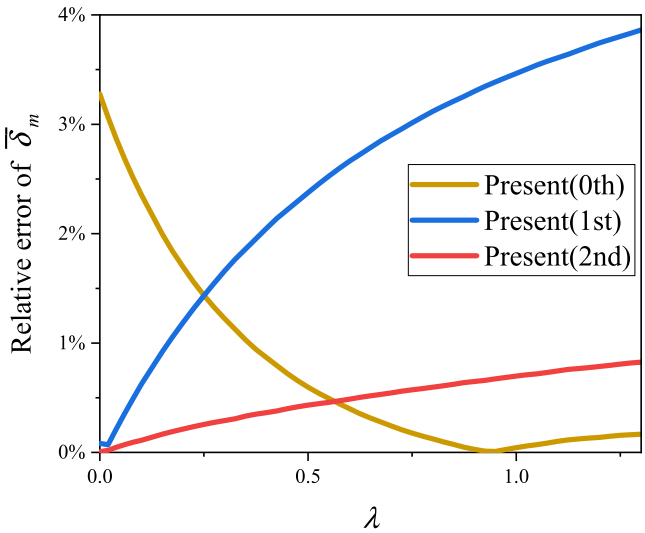

Fig. 5. Relative error of the analytical solutions of dimensionless maximum contact depth relative to the numerical solutions.

with its dimensionless counterpart:

$$\overline{F} = \frac{F}{k^{\frac{1}{3}} m_s^{\frac{2}{3}} V_0^{\frac{4}{3}}} = \overline{\delta}^2 \tag{34}$$

From Eq. (34), we conclude that the dimensionless maximum contact force by $\overline{F}_m = \overline{\delta}_m^2$, and $\overline{F}_m$ can be expressed in terms of λ. In addition, we also extracted the dimensionless total contact duration $\overline{t}_t$ and dimensionless compression duration $\overline{t}_c$. They are discussed in Appendix A4.The main results are as follows:

$$\overline{F}_m = \left(\lambda + \left(\frac{3}{2}\right)^{-2/3}\right)^{-1} \tag{35}$$

$$\overline{t}_t = 3.210\exp\left(0.476\lambda^{1.182}\right) \tag{36}$$

$$\overline{t}_c = 1.605\exp\left(-0.158\lambda^{0.697}\right) \tag{37}$$

Dimensionless duration multiplied by T gives the true duration.

The impact problem is under the assumption that "the reaction of plates to forces of such short duration that the waves reflected from the boundary may be neglected"(Zener, 1941). This means that the restitution of the spherical impactor should occur before the waves reflected from the plate's contour come to the center of impact. Thus the minimum radius of the plate is equal to half the waves propagation distance over the contact duration.

There are three types of wave:

- If the longitudinal wave is just reflected to the impact center, the radius of the plate r_0 should be equal to $r_P = 0.5\overline{t}_t T c_P$;
- if the shear wave is just reflected to the impact center, the radius of the plate r_0 should be equal to $r_S = 0.5\overline{t}_t T c_S$;
- if the Rayleigh wave is just reflected to the impact center, the radius of the plate r_0 should be equal to $r_R = 0.5\overline{t}_t T c_R$.

Where c_P, c_S and c_R are the velocities of longitudinal wave, shear wave and Rayleigh wave of the plate(Achenbach, 1975):

$c_P = \sqrt{\frac{E_2}{\rho_2}\frac{1-\nu_2}{(1+\nu_2)(1-2\nu_2)}}$, $c_S = \sqrt{\frac{E_2}{\rho_2}\frac{1}{2(1+\nu_2)}}$ and $c_R = \frac{0.862+1.14\nu_2}{1+\nu_2}c_S$.

$r_R < r_S < r_P$ because $c_R < c_S < c_P$.

In the finite element impact models, we took the radius of the plate as $r_0 < r_R$, $r_R \leqslant r_0 < r_S$, $r_S \leqslant r_0 < r_P$ and $r_P \leqslant r_0$, and fixed the edge of the plates. The FEM results of the contact depth-time are compared with the present theoretical solution, as shown in Fig. 6 (a). The contact history is almost the same as long as the radius of the plate r_0 is larger than r_R. When radius of the plate r_0 is less than the critical size r_R, however, the contact history will change as shown in Fig. 6 (a). This means that the Rayleigh wave reflection has a significant influence on the impact process, whereas the effects of longitudinal and shear waves are negligible.

Similar FEM simulations were performed on the bare plate (see Peng et al., 2021b for the contact duration), and the contact depth-time curves were compared with the Zener solution. The results are the same as those of the coated plate, as shown in Fig. 6 (b). Therefore, we can

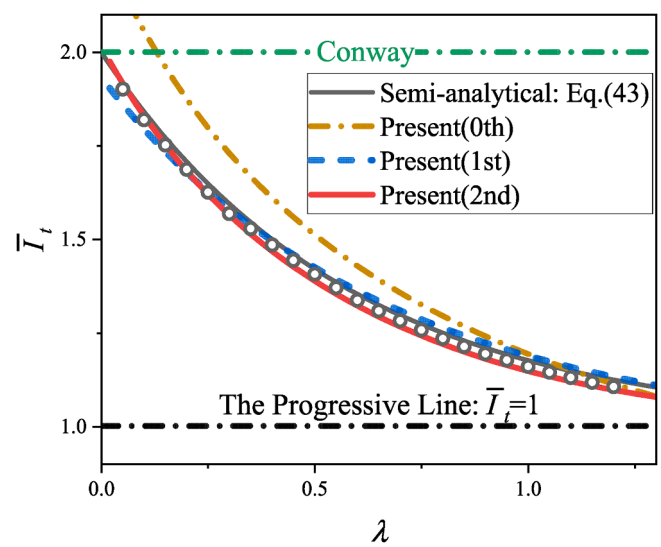

Fig. 7. Relationship between total impulse and dissipation factor λ.

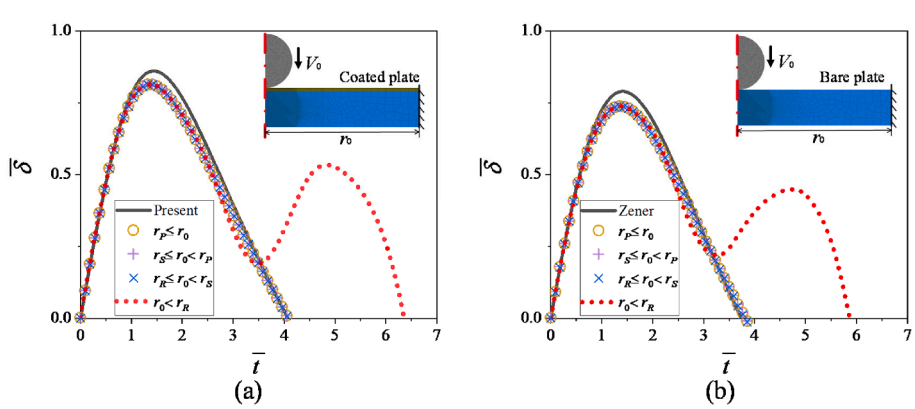

Fig. 6. Contact depth-time relationship under different plate radii ($\lambda = 0.6$).

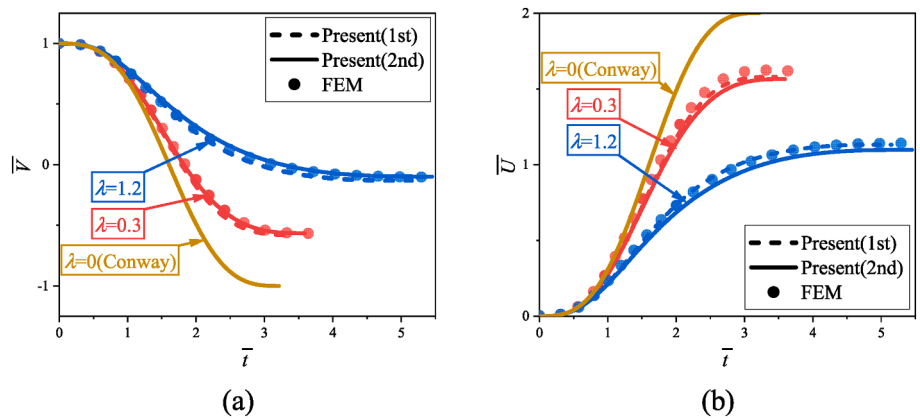

Fig. 8. History of (a) velocity of the sphere and (b) deflection of the center plate.

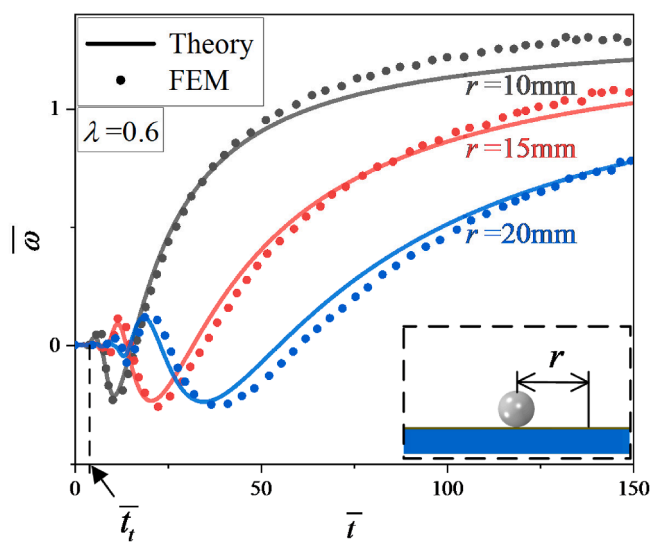

Fig. 9. Deflection response of the plate at the horizontal distance r from the force center (V_0=54.398m/s, h_1=0.05mm, h_2=0.3mm).

conclude that the Zener model and the present model are valid when the restitution of sphere occurs before the reflection of Rayleigh wave from boundary. The minimum distance between the boundary of the plate and the impact center is:

$$r_R = \frac{\bar{t}_t T c_R}{2} \tag{38}$$

3.2. Displacement history of sphere and plate

The impulse on the sphere can be obtained by the integral of contact force over time:

$$I(t) = \int_0^t F(t)\mathrm{d}t \tag{39}$$

Substituting Eqs. (13) and (34) yields:

$$I(\bar{t}) = \int_0^{\bar{t}} k^{\frac{1}{3}} m_s^{\frac{2}{3}} V_0^{\frac{4}{3}} \bar{F}\mathrm{d}(T\bar{t}) = m_s V_0 \int_0^{\bar{t}} \bar{F}\mathrm{d}\bar{t} \tag{40}$$

The dimensionless impulse can be defined as:

$$\bar{I}(\bar{t}) = \frac{I(\bar{t})}{m_s V_0} = \int_0^{\bar{t}} \bar{F}\mathrm{d}\bar{t} \tag{41}$$

and hence the dimensionless total impulse $\bar{I}_t$ reads:

$$\bar{I}_t = \bar{I}(\bar{t}_t) = \int_0^{\bar{t}_t} \bar{F}\mathrm{d}\bar{t} \tag{42}$$

The relationship between $\bar{I}_t$ and λ is shown in Fig. 7. For a conservative system, $\lambda = 0$, $\bar{I}_t$ reaches a maximum of 2. As λ increases, $\bar{I}_t$ decreases to 1. The 0th-order solution has relatively large error, but the 1st-order solution and the 2nd-order solution agree well with the FEM results. By fitting with least squares, we obtain an explicit expression:

$$\bar{I}_t = 1 + \exp(-1.730\lambda) \tag{43}$$

The velocity of the sphere $V(\bar{t})$ can be obtained by the following equation:

$$m_s V(\bar{t}) = m_s V_0 - m_s V_0 \bar{I}(\bar{t}) \tag{44}$$

We can define the dimensionless velocity as

$$\bar{V}(\bar{t}) = \frac{V(\bar{t})}{V_0} = 1 - \bar{I}(\bar{t}) \tag{45}$$

Similarly, the deflection of the plate center can be obtained (Zener, 1941):

$$U(\bar{t}) = \alpha I(\bar{t}) \tag{46}$$

and the dimensionless deflection is

$$\bar{U}(\bar{t}) = \frac{U(\bar{t})}{\alpha m_s V_0} = I(\bar{t}) \tag{47}$$

When the impact is completed, the deflection of the plate center can be given according to the total impulse Eq. (43).

With the present solution, we can plot the velocity history of sphere, as shown Fig. 8(a). When in the case of Conway solution ($\lambda = 0$), the coefficient of restitution is 1. As λ increases, the rebounding velocity of sphere becomes smaller. When λ is larger than 1.2, the rebounding velocity is less than $V_0/10$, more than 99% of the kinetic energy is dissipated by the flexural waves of the plate.

The history of center deflection of plate can be also well predicted by the proposed solution, as shown in Fig. 8(b). It is shown that the 1st-order solution can provide high accuracy, with relative error to FEM results less than 3%. It should be noted that, when $\lambda = 0$, the figure shows that the dimensionless deflection changes the most; however, when $\lambda = 0$, the bending rigidity of the plate tends to be infinite, and the true deflection is 0. As a result, Fig. 8(b) cannot directly reflect the real deflection of the plate. However, We can easily calculate the true deflection at the impact position of the coated plate using Eq. (47).

Using the force history, we can also calculate the deflection history of any location on the plate. The history of plate deflection at the horizontal distance r from the center due to a concentrated force at the center is provided by Sneddon (Sneddon, 1951), article 20.3:

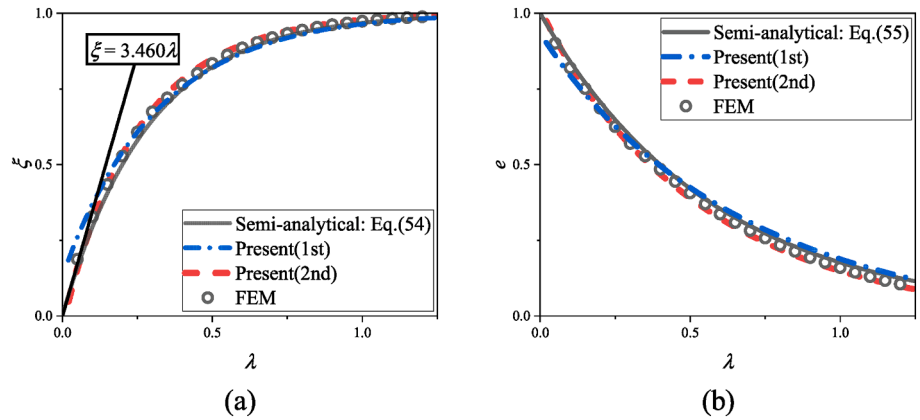

Fig. 10. (a) Relationship between ratio of energy loss of sphere and dissipation factor; (b) Relationship between coefficient of restitution and dissipation factor.

Table 1
General solution for impact of coated plate.

Deep impact ($\delta_m > \delta_{cr}$)	Shallow impact ($\delta_m \le \delta_{cr}$)
$\lambda = \frac{\pi}{8 \bullet 3^{1/6}} \gamma^{\frac{1}{3}} \left(\frac{V_0}{V}\right)^{\frac{1}{3}} \left(\frac{\rho_s}{\rho_2}\right)^{\frac{2}{3}} \left(\frac{E'_1}{E'_2}\right)^{\frac{1}{3}} \left(\frac{R}{h_2}\right)^2 \left(\frac{R}{h_1}\right)^{\frac{1}{3}} \left(1+\frac{3h_1E'_1}{h_2E'_2}\right)^{-\frac{1}{2}} \left(1+\frac{\rho_1 h_1}{\rho_2 h_2}\right)^{-\frac{1}{2}}$	$\lambda^* = \frac{\pi^{3/5}}{3^{1/2}} \left(\frac{V_0}{V}\right)^{\frac{1}{5}} \left(\frac{\rho_s}{\rho_2}\right)^{\frac{3}{5}} \left(\frac{E'_1}{E'_2}\right)^{\frac{2}{5}} \left(\frac{R}{2h_2}\right)^2 \left(1+\frac{3h_1E'_1}{h_2E'_2}\right)^{-\frac{1}{2}} \left(1+\frac{\rho_1 h_1}{\rho_2 h_2}\right)^{-\frac{1}{2}}$
$T = \left(\frac{2h_1 m_s}{\pi\gamma R V_0 E'_1}\right)^{1/3}$	$T^* = \left(\frac{3m_s}{4E'_1}\right)^{2/5} (RV_0)^{-1/5}$
$\delta_m = TV_0 \cdot \left(\lambda + 1.5^{-2/3}\right)^{-1/2}$	$\delta_m^* = T^* V_0 \cdot \left(\lambda^* + 1.25^{-3/5}\right)^{-2/3}$
$F_m = \frac{\gamma\pi E'_1 R}{2h_1}\delta_m^2$	$F_m^* = \frac{4}{3} R^{1/2} E'_1 \delta_m^{*3/2}$
$t_t = T \cdot 3.210 \exp\left(0.476\lambda^{1.182}\right)$	$t_t^* = T^* \cdot 3.214 \exp\left(0.23\lambda^{*1.80}\right)$
$I_t = m_s V_0 [1 + \exp(-1.730\lambda)]$	$I_t^* = m_s V_0 [1 + \exp(-1.378\lambda^*)]$
$\xi = 1 - \exp(-3.460\lambda)$	$\xi^* = 1 - \exp(-2.755\lambda^*)$
$e = \exp(-1.730\lambda)$	$e^* = \exp(-1.378\lambda^*)$
$\omega(r,t) = \begin{cases} \frac{2\alpha I_t}{\pi t_t}\left[tH\left(\frac{r^2/32}{\alpha Dt}\right)\right] & t \le t_t \\ \frac{2\alpha I_t}{\pi t_t}\left[tH\left(\frac{r^2/32}{\alpha Dt}\right) - (t-t_t)H\left(\frac{r^2/32}{\alpha D(t-t_t)}\right)\right] & t > t_t \end{cases}$	$\omega^*(r,t) = \begin{cases} \frac{2\alpha I_t^*}{\pi t_t^*}\left[tH\left(\frac{r^2/32}{\alpha Dt}\right)\right] & t \le t_t^* \\ \frac{2\alpha I_t^*}{\pi t_t^*}\left[tH\left(\frac{r^2/32}{\alpha Dt}\right) - (t-t_t^*)H\left(\frac{r^2/32}{\alpha D(t-t_t^*)}\right)\right] & t > t_t^* \end{cases}$
Where, $D = \frac{2}{3}h_2^3 E'_2 \left(1+\frac{3h_1E'_1}{h_2E'_2}\right)$ and $\alpha = \frac{(3\rho_2/E'_2)^{1/2}}{16\rho_2 h_2^2}\left(1+\frac{3h_1E'_1}{h_2E'_2}\right)^{-1/2}\left(1+\frac{\rho_1 h_1}{\rho_2 h_2}\right)^{-1/2}$	

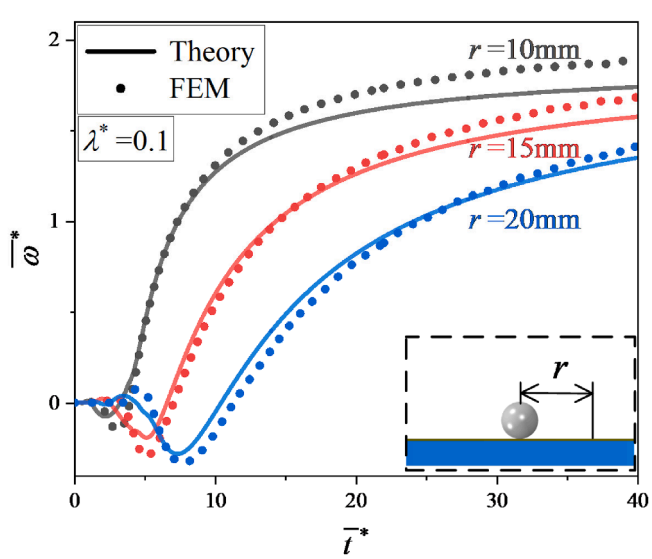

Fig. 11. Deflection response of the plate at the horizontal distance r from the force center (V_0=0.2m/s, h_1=0.05mm, h_2=0.3mm).

$$\omega(r,t) = \frac{2\alpha}{\pi}\int_0^t \left[\int_0^u F(\tau)\mathrm{d}\tau\right] \sin\left[\frac{r^2/32}{\alpha D(t-u)}\right] \frac{\mathrm{d}u}{t-u} \tag{48}$$

Medick found that the plate deflection is insensitive to the detailed force history, but highly correlated with the total impulse (Medick, 1961). Assuming that the force during contact is constant and equal to the total impulse divided by the contact time, we can get the expression of plate deflection with respect to total impulse I_t and total contact duration t_t:

$$\omega(r,t) = \begin{cases} \frac{2\alpha I_t}{\pi t_t}\left[tH\left(\frac{r^2/32}{\alpha Dt}\right)\right] & t \leqslant t_t \\ \frac{2\alpha I_t}{\pi t_t}\left[tH\left(\frac{r^2/32}{\alpha Dt}\right) - (t-t_t)H\left(\frac{r^2/32}{\alpha D(t-t_t)}\right)\right] & t > t_t \end{cases} \tag{49}$$

where:

$H(x) = \pi/2 - \mathrm{Si}(x) + x\mathrm{Ci}(x) - \sin(x)$, $\mathrm{Si}(x) = \int_0^x \frac{\sin t}{t}\mathrm{d}t$, and $\mathrm{Ci}(x) = \int_{+\infty}^x \frac{\cos t}{t}\mathrm{d}t$.

The dimensionless plate deflection can be defined as

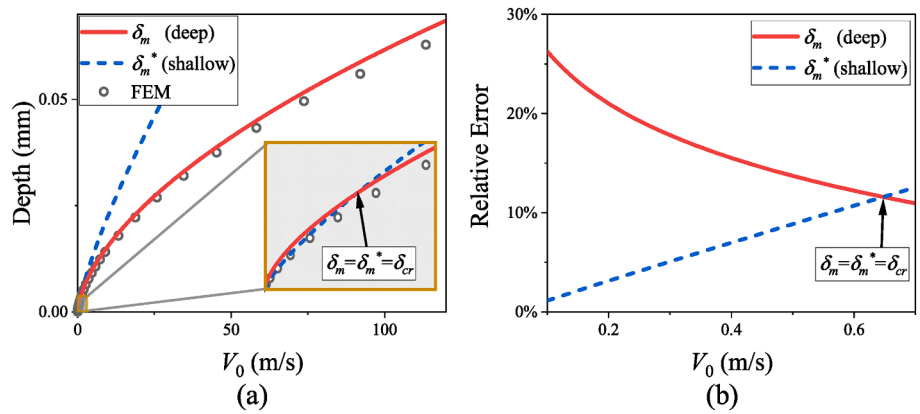

Fig. 12. (a)Maximum contact depth of deep impact ($\delta_m > \delta_{cr}$) and shallow impact ($\delta_m \le \delta_{cr}$); (b) Relative error at small speed (E_1=6GPa,E_2=72GPa,h_1=0.05mm, h_2=0.3mm,R=0.9mm).

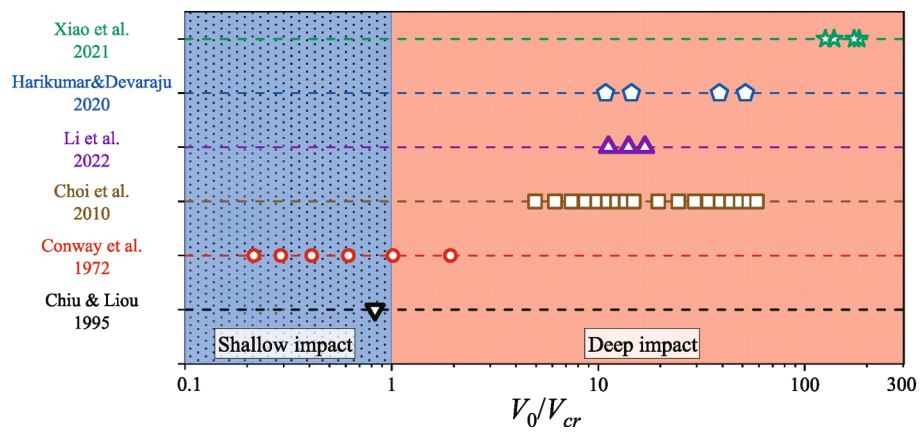

Fig. 13. Application range of our impact model (V_0 denotes the initial velocity).

$$\overline{\omega}(r,\bar{t}) = \frac{\omega(r,\bar{t})}{\alpha m_s V_0} = \begin{cases} \dfrac{2\bar{I}_t}{\pi \bar{t}_t}\left[\bar{t}\mathrm{H}\left(\dfrac{r^2/32}{\alpha DT\bar{t}}\right)\right] & \bar{t} \leqslant \bar{t}_t \\ \dfrac{2\bar{I}_t}{\pi \bar{t}_t}\left[\bar{t}\mathrm{H}\left(\dfrac{r^2/32}{\alpha DT\bar{t}}\right) - (\bar{t}-\bar{t}_t)\mathrm{H}\left(\dfrac{r^2/32}{\alpha DT(\bar{t}-\bar{t}_t)}\right)\right] & \bar{t} > \bar{t}_t \end{cases} \tag{50}$$

where $\bar{t}_t$ and $\bar{I}_t$ are given by Eqs. (36) and (43) respectively.

The comparison with FEM results is shown in Fig. 9, and validates Eq. (50) has a high accuracy. It is shown that the bending wave generates from the center of impact. When $\bar{t} > \bar{t}_t$, the deflections at different locations response in a similar way, and the characteristic wavelength is proportional to r^2. With enough long time, the deflections at different locations of the plate approach the same maximum $\bar{I}_t$.

3.3. Energy dissipation and coefficient of restitution

With the final velocity of V_F, the sphere ends the impact when $t = t_t$. The kinetic energy loss of sphere can be calculated by $W = m_s(V_0^2 - V_F^2)/2$. The ratio of energy loss of sphere is:

$$\xi = \frac{W}{\frac{1}{2}m_s V_0^2} = 1 - \left(\frac{V_F}{V_0}\right)^2 = 1 - \overline{V}_F^2 \tag{51}$$

With $\overline{V}_F = 1 - \bar{I}_t$ from Eq. (45), we can obtain the ratio of energy loss of sphere:

$$\xi = 2\bar{I}_t - \bar{I}_t^2 \tag{52}$$

Next, we will solve the coefficient of restitution e, as in Eq. (9). Eq. (46) shows that the displacement of the plate center is proportional to the impulse of the contact force. With the fact that the velocity at the center of the plate is 0 before and after impact, we can calculate e by:

$$e = -\frac{V_F}{V_0} = -\overline{V}_F = \bar{I}_t - 1 \tag{53}$$

Substituting Eq. (43) into Eqs. (52) and (53) yields the following explicit expressions for ξ and e:

$$\xi = 1 - \exp(-3.460\lambda) \tag{54}$$

$$e = \exp(-1.730\lambda) \tag{55}$$

As shown in Fig. 10, the semi-analytical solution agrees well with the FEM results, with relative error less than 5% when $\lambda > 0.2$. For a case with small λ, the bending stiffness of plate is so high that the dissipation rate is close to 0. By Taylor series, Eq. (54) can be expanded at $\lambda = 0$ as

$$\xi = 3.460\lambda \tag{56}$$

which shows how fast the energy dissipation grows with λ.

Fig. 10 also confirms that the ratio of energy loss of sphere near the origin is proportional to λ. When $\lambda \leqslant 0.028$, the relative error between Eq. (56) and Eq. (54) is less than 5%. In this case, the relationship between ratio of energy loss of sphere and physical parameters is obtained by substituting Eq. (19) into Eq. (56):

$$\xi = 1.131\gamma^{\frac{1}{3}}\left(\frac{V_0}{V'}\right)^{\frac{1}{3}}\left(\frac{\rho_s}{\rho_2}\right)^{\frac{2}{3}}\left(\frac{E_1'}{E_2'}\right)^{\frac{1}{3}}\left(\frac{R}{h_2}\right)^2\left(\frac{R}{h_1}\right)^{\frac{1}{3}}\left(1+\frac{3h_1E_1'}{h_2E_2'}\right)^{-\frac{1}{2}}\left(1+\frac{\rho_1h_1}{\rho_2h_2}\right)^{-\frac{1}{2}} \tag{57}$$

Therefore, when a sphere impacts a plate coated soft film, the ratio of energy loss of sphere ξ is proportional to V_0 to the power of 1/3, different from Peng et al.'s result (Peng et al., 2021b) where the ratio of energy

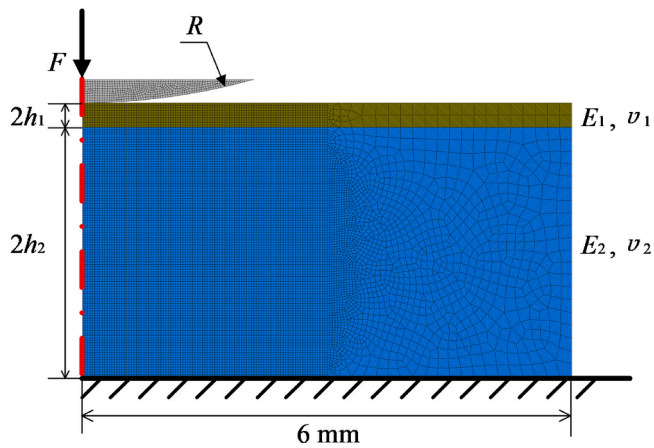

Fig. A1. Axisymmetric FEM model of static contact between sphere and the plate coated with soft film.

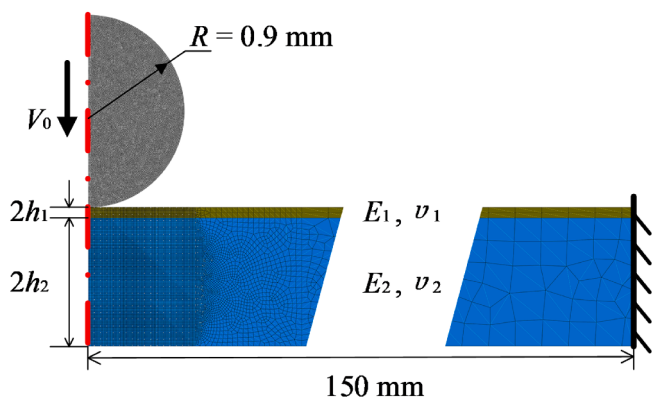

Fig. A2. Axisymmetric FEM model of impact of sphere on the plate coated with soft film.

loss of a sphere impacting on a plate without coatings is proportional to V_0 to the power of 1/5.

Both results are obtained when the dissipation factor λ is close to 0, which corresponds to the case that thickness or rigidity of the plate is relatively large. Compared with the impact of the sphere on the bare plate, the change of kinetic energy loss caused by the change of impact speed is more obvious when the sphere impacts on the plate with soft coating. The reason is that in Hertz contact relationship and Conway contact relationship, the sensitivity of contact force change caused by the change of contact depth is different, which makes the relationship between the dimensionless dissipation factor λ and impact velocity different when we non-dimensionalize the control equations.

In fact, the two theories should be changed gradually rather than suddenly. Dimitriadis et al. (2002) tried to solve this problem, they only got the solution of Hertz's model to a relatively shallow contact ($\delta < (2h_1)^2/R$), but could not switch to Conway's model.

3.4. General solution for impact of coated plate

In the above section, we have studied the deep impact ($\delta_m > \delta_{cr}$) of a sphere on a coated plate, and have obtained expressions for dissipation factor, depth history, contact force history and etc. With our previous study on sphere/plate impact (Peng et al., 2021b), we can draw a complete picture for the impact of coated plate, shallow or deep. The results are gathered in Table 1.

The results of the shallow impact ($\delta_m \le \delta_{cr}$) theory using Hertz contact theory have been discussed in our previous work (Peng et al., 2021b), but not the deflection response of plates. In this study, we further provided the theoretical deflection of plate under shallow impact ($\delta_m \le \delta_{cr}$), as shown in Fig. 11, where $\overline{\omega}^* = \omega^*/(\alpha m_s V_0)$ and $\overline{t}^* = t/T^*$ are dimensionless plate deflection and dimensionless time under shallow impact ($\delta_m \le \delta_{cr}$), respectively. The prediction of shallow impact ($\delta_m \le \delta_{cr}$) theory agrees well. Moreover, the closer to the impact center, the valley of the deflection curve will be shallower. We can know from Fig. 8 (b) that when $r = 0$, the deflection curve will degenerate into a monotonically increasing shape, that is, the valley of the deflection curve disappears. Since the closer to the impact center, the more obvious the constraint of contact on deflection.

Table A1
Material parameters of the model.

	Sphere	Film	Plate
Young's Modules (GPa)	∞	$E_1 = 4$	$E_2 = 72$
Poisson Ratio	/	$\nu_1 = 0.21$	$\nu_2 = 0.21$
Density (kg/m^3)	$\rho_s = 2500$	$\rho_1 = 1200$	$\rho_2 = 2500$

Table A2
Plate thickness and initial velocity corresponding to different dissipation factors λ.

λ	h_2 (mm)	V_0 (m/s)
0.05	0.8	10.277
0.10	0.6	14.923
0.15	0.4	4.597
0.20	0.4	10.896
0.25	0.4	21.281
0.30	0.3	36.773
0.35	0.3	10.798
0.40	0.3	16.118
0.45	0.3	22.949
0.50	0.3	31.480
0.55	0.3	41.900
0.60	0.3	54.398
0.65	0.25	23.871
0.70	0.25	29.814
0.75	0.25	36.670
0.80	0.25	44.504
0.85	0.25	53.381
0.90	0.25	63.367
0.95	0.22	35.464
1.00	0.22	41.364
1.05	0.22	47.884
1.10	0.22	55.056
1.15	0.22	62.909
1.20	0.22	71.477

3.5. Velocity dependent impact model

For the indentation of a sphere onto a plate with soft coatings, on the one hand, if the contact depth is shallow, the influence of the plate on the stress field in the soft coating can be ignored. The stress distribution is the same as that of the half-space contact, and the Hertzian contact theory $F = 4E'_1 R^{1/2}\delta^{3/2}/3$ is applicable. In such case, the corrected Conway's contact theory $F = \gamma\pi E'_1 R\delta^2/(2h_1)$ with quadratic force-depth relationship underestimates the contact force. On the other hand, if the contact depth exceeds a certain value (the critical contact depth in the present study), the influence of the plate with higher modulus on the stress field of the soft coating cannot be ignored. The stress gradually distributed uniformly along the thickness of coating, where Conway's contact theory is applicable and Hertz theory underestimates the contact force. In sum, with the increase of contact depth, the relationship between contact force and contact depth changes from Hertz's theory to Conway's theory, which, in turn, dictates different amount of energy dissipated by the flexural wave.

For the dynamic impact problem in the present study, the deformation of plate, as the result of the contact force on plate, accompanies the

impinging process. The way the contact force builds up is associated with the critical contact depth. As we show in the manuscript, when the sphere is pressed to this critical depth, the work of the contact force calculated by Hertz model and Conway model are equal. If the actual contact depth does not reach the critical depth, Hertz contact theory is more accurate, otherwise, Conway contact theory.

The impact depth depends on the initial velocity, thus it remains a question: how does the initial velocity dictates the choice of impact models? In this section, we discuss such critical velocity in aspect of energy balance.

When a rigid sphere impacts a plate coated with soft film, the critical depth for the transition of the two models is obtained when the work done by the contact forces of the two theories is equal. Equating $\int_0^{\delta_{cr}} \gamma\pi E_1' R\delta^2/(2h_1)\mathrm{d}\delta$ to $\int_0^{\delta_{cr}} 4E_1' R^{1/2}\delta^{3/2}/3\mathrm{d}\delta$, the critical depth δ_{cr} for the choice of two models for deep and shallow impacts is obtained as follows:

$$\delta_{cr} = \frac{64}{25\pi^2\gamma^2}\frac{(2h_1)^2}{R} \tag{58}$$

Zener used Hertz contact model to solve the dynamic impact problem of the sphere plate system. For the dynamic impact of sphere on a coated plate, Zener's theory can only be applied in cases where the maximum impact depth is less than or equal to δ_{cr}.

According to Table 1, the maximum impact depth depends on the impact velocity of the sphere, and comparison with the FEM results (see Appendix A1 for details) is shown in Fig. 12(a). Conway contact theory is used under deep contact and Hertz contact theory is used under shallow contact. Fig. 12(b) shows the relative error of the two impact models at low speed. The error of the deep impact model at low speed exceeds 20%, which decreases with the increase of speed. When the maximum impact depth is greater than δ_{cr}, the deep impact model has smaller error. In another words, when $\delta_m > \delta_{cr}$, we have to use the deep impact $(\delta_m > \delta_{cr})$ model; while when $\delta_m \leqslant \delta_{cr}$, we have to use the shallow impact $(\delta_m \leq \delta_{cr})$ model. In this sense, we can obtain the critical velocity by equating δ_m to δ_{cr}:

$$\delta_m = \delta_{cr} \tag{59}$$

Substituting Eqs. (12), (23) and (58) into Eq. (59), we have:

$$\frac{TV_0R\gamma^2}{(2h_1)^2}\cdot\left(\lambda + \left(\frac{3}{2}\right)^{-2/3}\right)^{-1/2} = \frac{64}{25\pi^2} \tag{60}$$

Solving Eq. (60), we obtain an expression for the critical impact velocity V_{cr}:

$$V_{cr} = \left(\sqrt{2y_0} + \sqrt{-2y_0 - 2\varphi\Big/\sqrt{2y_0}}\right)^3\Big/8 \tag{61}$$

where, y_0 and φ are material-dependent coefficients:

$$y_0 = \left(\frac{\varphi^2}{16} + \sqrt{\left(\frac{\varphi^2}{16}\right)^2 - \left(\frac{\mu}{3}\right)^3}\right)^{1/3} + \left(\frac{\varphi^2}{16} - \sqrt{\left(\frac{\varphi^2}{16}\right)^2 - \left(\frac{\mu}{3}\right)^3}\right)^{1/3}$$

$$\varphi = -\left(\frac{8}{5\pi}\right)^4\frac{\alpha k(2h_1)^4}{\gamma^4R^2}$$

and

$$\mu = -\left(\frac{8}{5\pi}\right)^4\frac{(2h_1)^4}{\gamma^4R^2}\left(\frac{2k}{3m_s}\right)^{2/3}$$

When the geometrical and material parameters of the sphere and coated plate are known a priori, the critical velocity can be calculated by using Eq. (61). For an impact velocity greater than V_{cr}, the theory of deep impact $(\delta_m > \delta_{cr})$ applies, and otherwise applies the theory of shallow impact $(\delta_m \leq \delta_{cr})$.

In Fig. 13, we put the previous experiments of sphere impact on

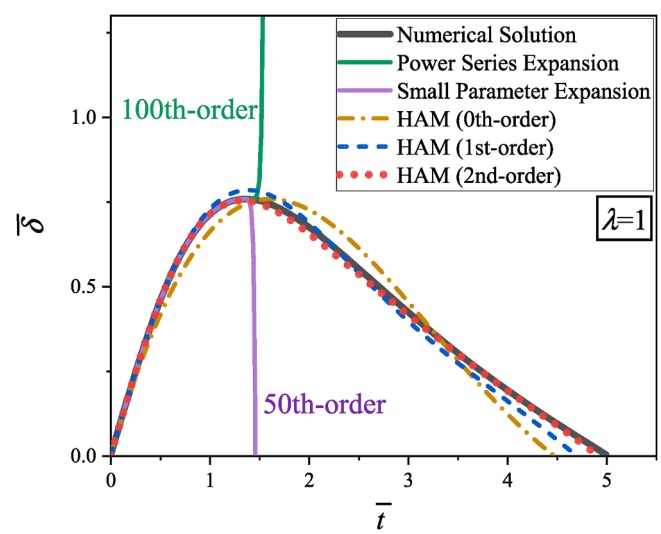

Fig. A4. Solutions of Power Series Expansion Method, Small Parameter Expansion Method and Homotopy Analysis Method.

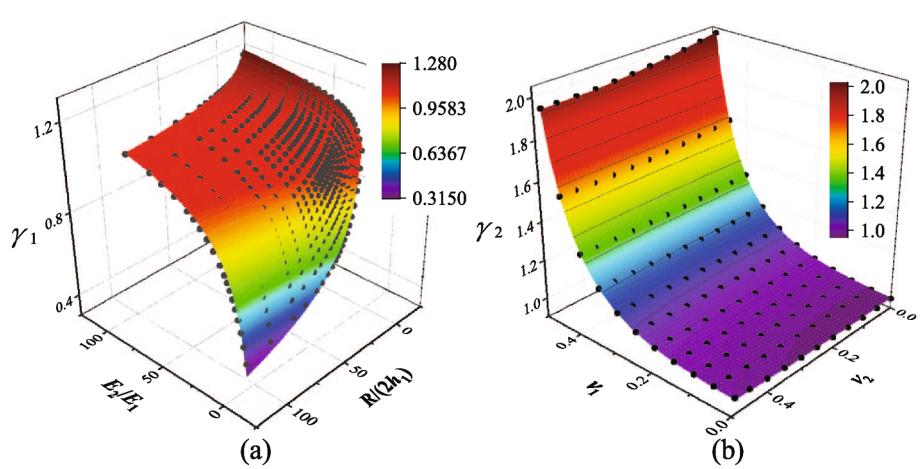

Fig. A3. (a) The relationship between the correction coefficient γ_1 about E_2/E_1 and $R/(2h_1)$; (b) The relationship between the correction coefficient γ_2 about Poisson's ratios. (the dots represent FEM results and the surfaces are fitted).

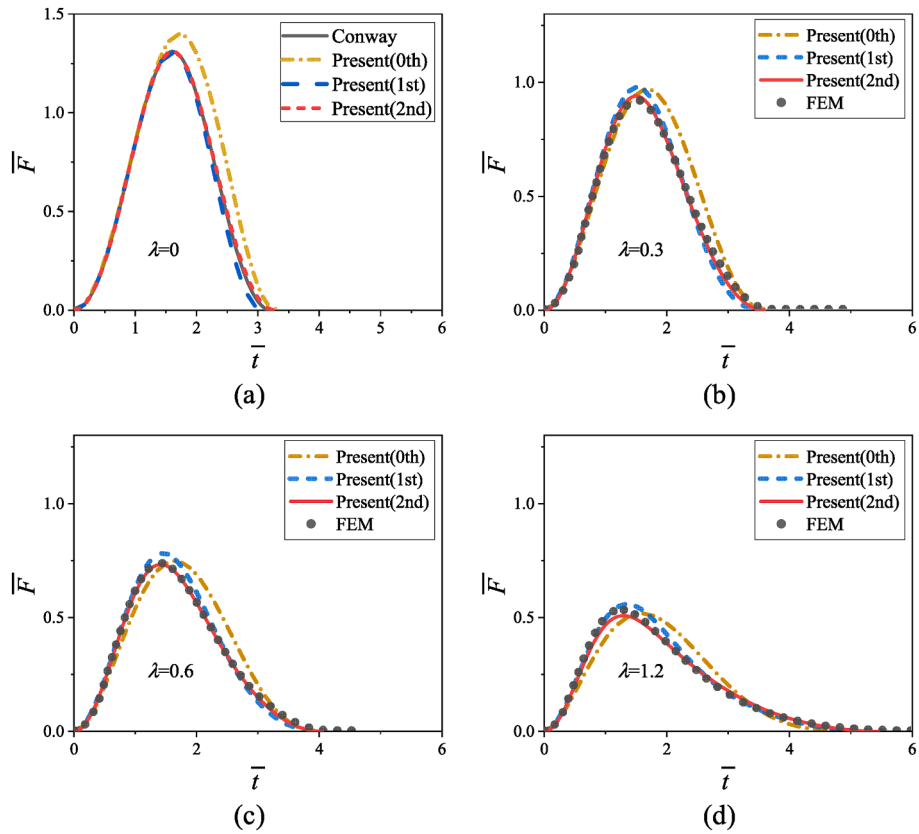

Fig. A5. Analytical solution and FEM results of contact force–time: (a)λ=0; (b)λ=0.3; (c)λ=0.6; (d)λ=1.2.

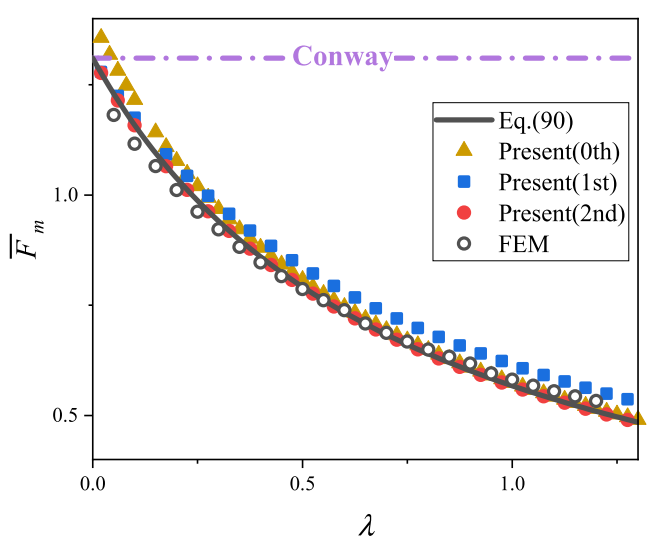

Fig. A6. Relationship between maximum contact force and dissipation factor.

coated plates in the phase diagram, where the abscissa shows the applicable ranges of models. It is shown that most of these experiments are within the range of deep impact ($\delta_m > \delta_{cr}$) model. Chiu and Liou's experiments (Chiu and Liou, 1995) explored the initial fracture of the brittle coating itself, and the impact velocity was small enough to apply to the theory of shallow impact ($\delta_m \leq \delta_{cr}$). However, most of the experiments are interested in the deep impact ($\delta_m > \delta_{cr}$) response of the coated plate, such as Choi et al. (Choi et al., 2010), Xiao et al. (Xiao et al., 2021), Li et al. (Li et al., 2022), Harikumar and Devaraju (Harikumar and Devaraju, 2020). Therefore, the deep impact ($\delta_m > \delta_{cr}$) model is applicable in a more general scope. It is worth mentioning that the impact velocities of Conway et al.'s experiments are just around the critical value, and the experimental results (Fig. 5 of (Conway et al., 1972)) prove the correctness of our phase diagrams.

3.6. Limitation of present model

For the prediction of the deflection history at any position on the plate, Eq. (50) can only describe the deflection history far away from the impact center. The reason is that the contact force is can no longer viewed as a concentration force in the vicinity of impact center. In addition, for the indention of thin films, the strain gradient effect (Nix and Gao, 1998; Saha et al., 2001), indentation size effect (Huang et al., 2006) might be significant, which will be investigated in our future study. In addition, the contact of sphere may introduce some other factors, such as contact plasticity (Peng et al., 2021a; Wang et al., 2017), viscosity (Carretero-González et al., 2009; Vergara, 2010), these factors are not studied in present work. Also, the interface adhesion has not been considered in this work, while a recent study (Peng et al., 2020) has shown that the pull-off force of a rigid punch from an elastic film has a strong thickness dependence. Similar to previous studies that solitary wave on chain can be used to evaluate the plate thickness (Job et al., 2005; Peng et al., 2022), the present model can also pave the way for non-destructive evaluation of coating thickness.

4. Conclusion

For the impact problem of coated plate, we proposed a modified Conway's model for force–displacement relationship, and further a dynamical equation for the impact process. Using homotopy analysis method, we proposed an analytical solution to such equation to predict the elastic impact between a rigid sphere and a coated plate. Using the obtained contact force history, we studied the energy loss due to the flexural wave, as well as the motion of the sphere and plate during the

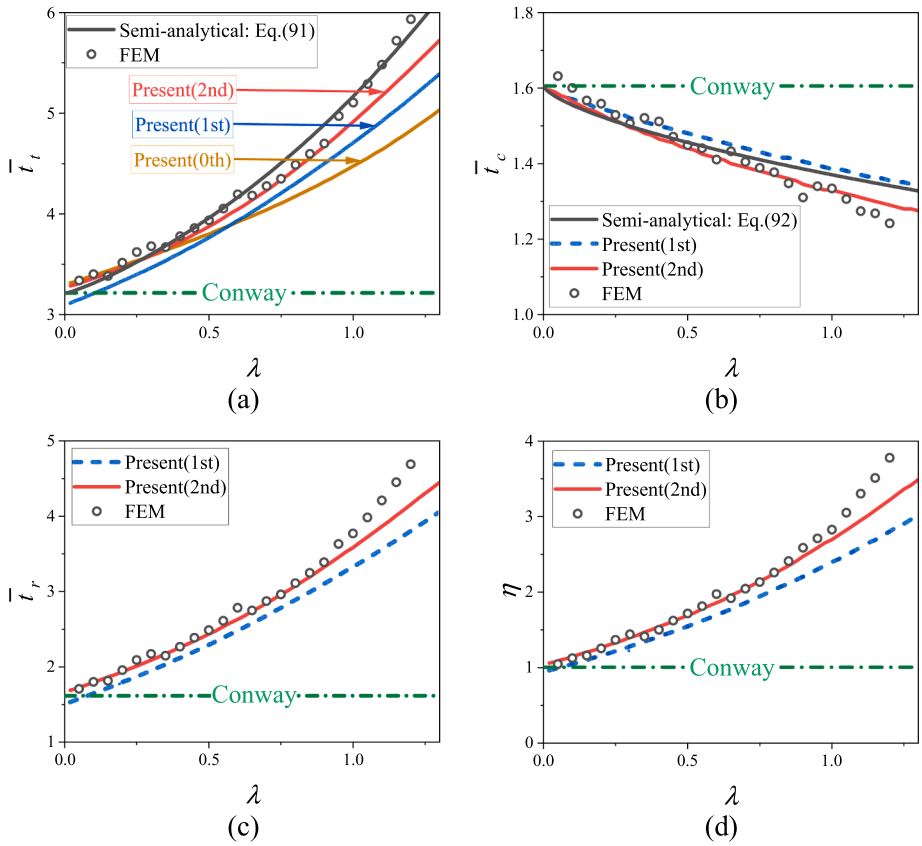

Fig. A7. Relationship between contact duration and dissipation factor: (a) $\bar{t}_t$; (b) $\bar{t}_c$; (c) $\bar{t}_r$; (d) η.

impact. The conclusions are as follows:

(1) We obtained an explicit expression for the history of contact force up to any order of the homotopy embedding parameter. By comparing with numerical solution and FEM, we concluded that present zeroth-order and first-order solutions can provide enough accuracy, with the relative error less than 3.3% and 3.9%, respectively.
(2) Using the present solution, we derived an expression for energy dissipation and coefficient of restitution, revealing that the energy loss is proportional to the impact velocity to the power of 1/3 for coated plate, instead of to the power of 1/5 for bare plate.
(3) Joining with our preview study on bare plate impact, we provided a complete set of models for impact of coated plate, and further, a criterion for the selection of models. We derived a critical velocity, above which the model for deep impact ($\delta_m > \delta_{cr}$) applies, and below which the model for shallow impact ($\delta_m \leq \delta_{cr}$) applies.

Declaration of Competing Interest

The authors declare that they have no known competing financial interests or personal relationships that could have appeared to influence the work reported in this paper.

Data availability

Data will be made available on request.

Acknowledgement

This work was supported by the National Natural Science Foundation of China (No. 12022210, 12032001), by the Youth Innovation Promotion Association CAS (2018022). This work was also supported by the National Natural Science Foundation of China, Basic Science Center Program for "Multiscale Problems in Nonlinear Mechanics" (No.11988102), and by the National Key Research Development Program of China (No. 2020-JCJQ-ZD-254)

Appendix

A1. FEM model

For static contact, we use the Abaqus/Standard analysis module. The axisymmetric model is established as shown in Fig. A1. The sphere is rigid, hence it is only necessary to model the sphere crown in the contact area (as shown in gray in Fig. A1). Define tie constraint between film and plate. Limit all displacements at the bottom of the plate. Keep the thickness and Young's modulus of the soft film unchanged: $2h_1 = 0.1$mm, $E_1 = 4$Gpa; Change the radius of the sphere and Young's modulus of the plate: $R/(2h_1) \in [2, 100]$, $E_2/E_1 \in [6, 100]$; Set the plate thickness greater than twice the maximum contact radius; Poisson's ratio $\nu_1 = \nu_2 = 0.21$; The radius of the coated plate is set to 6 mm. The analysis step is Static/General. The normal behavior between the rigid sphere and the film is set as hard contact, the tangential behavior is set as penalty, and the friction coefficient is 0.01. The approximate size of the grid in the contact area is 0.01 and the grid type is CAX4R. The contact depth δ and contact force F during static indentation of

a rigid sphere into the film are obtained by applying displacement load to the rigid sphere.

For dynamic impact, we still use the Abaqus/Standard analysis module. Fig. A2 plots the axisymmetric model. The inertia force of the sphere is considered in the dynamic collision process, so the whole sphere is modeled as shown in Fig. A2 grey, the radius R of the sphere is 0.9 mm; The film thickness $2h_1$ is 0.1 mm and is bound to the plate. The radius of the coated plate is large enough (150 mm) to prevent the flexural waves from reflecting back. The analysis step is dynamic implicit. The normal phase behavior between the rigid sphere and the film is set as hard contact, the tangential behavior is set as penalty, and the friction coefficient is 0.01. The approximate size of the grid in the contact area is 0.01 and the grid type is CAX4R. Initial velocity load V_0 is applied to the rigid sphere and dissipation factor λ is changed by changing plate thickness $2h_2$ and initial velocity V_0. The relevant physical parameters are listed in Table A1 and Table A2.

A2. Correction coefficient to Conway's static indentation model

We conduct simulation simulations on static contact according to Appendix A1. The FEM results of contact force and the results of Eq. (2) are obtained when the indentation depth meets $\delta/(2h_1) = 0.4$. The ratio of the two is the correction coefficient γ. The coupling effect between Poisson's ratios and other parameters is small. Considering the operability of fitting, we decouple Poisson's ratios and other parameters. Therefore, the correction factor can be expressed as:

$$\gamma = \gamma_1\gamma_2 \tag{62}$$

γ_1 is a function of E_2/E_1 and $R/(2h_1)$, γ_2 is a function of ν_1 and ν_2. Keep the values of ν_1 and ν_2 equal to 0.21, and then the value of γ_2 is taken as 1. The relationship between the correction coefficient and E_2/E_1 and $R/(2h_1)$ is shown in Fig. A3(a). γ_1 tends to 1 with the increase of E_2/E_1 and $R/(2h_1)$. By fitting:

$$\gamma_1 = G_1 + G_2\left(\frac{E_2}{E_1}\right)^{G_5} + G_3\left(\frac{R}{2h_1}\right)^{G_6} + G_4\left(\frac{E_2}{E_1}\right)^{G_5}\left(\frac{R}{2h_1}\right)^{G_6} \tag{63}$$

Where

$$G_1 = 5.9798 \quad G_2 = -283.54876 \quad G_3 = -4.60697$$
$$G_4 = 283.17337 \quad G_5 = -0.41051 \quad G_6 = -0.00146$$

The fitting has high accuracy, the coefficient of determination: COD = 0.9965.

When both of the ratios $R/(2h_1)$ and E_2/E_1 are greater than 100, we will take $\gamma_1 = 1$;

When one of the ratios $R/(2h_1)$ or E_2/E_1 is greater than 100, we will take this ratio as 100.

We have tested this treatment, and result shows well agreement with FEM.

Keep $E_2/E_1 = 18$ and $R/(2h_1) = 9$, then $\gamma_2 = 0.996$ from Eq. (63). The relationship between γ_1 and Poisson's ratios is shown in Fig. A3(b). The influence of the Poisson's ratio of the plate is very small, and the influence of the Poisson's ratio of the coating mainly occurs in the range of close to 0.5. By fitting:

$$\gamma_2 = \frac{g_1 + g_2\nu_1 + g_3\nu_2 + g_4\nu_2^2 + g_5\nu_2^3}{1 + g_6\nu_1 + g_7\nu_1^2 + g_8\nu_1^3 + g_9\nu_2 + g_{10}\nu_2^2} \tag{64}$$

where

$$g_1 = 0.95458 \quad g_2 = -0.86196 \quad g_3 = 0.04125 \quad g_4 = 0.13038 \quad g_5 = 0.03515$$
$$g_6 = -1.00497 \quad g_7 = 0.02758 \quad g_8 = -2.13816 \quad g_9 = 0.06728 \quad g_{10} = 0.02767$$

The fitting also has high accuracy, the coefficient of determination: COD = 0.9999.

A3. Homotopy analysis method for Eq. (15)

Define nonlinear operators:

$$\mathscr{N}(\bar{\delta}) = \frac{\mathrm{d}^2\bar{\delta}}{\mathrm{d}\bar{t}^2} + 2\lambda\bar{\delta}\frac{\mathrm{d}\bar{\delta}}{\mathrm{d}\bar{t}} + \bar{\delta}^2 \tag{65}$$

Define linear operators:

$$\mathscr{L}(\bar{\delta}) = \frac{\mathrm{d}^2\bar{\delta}}{\mathrm{d}\bar{t}^2} + \mathrm{A}\bar{\delta}_{\mathrm{m}}\frac{\mathrm{d}\bar{\delta}}{\mathrm{d}\bar{t}} + \mathrm{B}\bar{\delta}_{\mathrm{m}}\bar{\delta} \tag{66}$$

Where A and B are the coefficients to be selected. In order to make the shape of the solution of the linear equation $\mathscr{L}(\bar{\delta}) = 0$ and the solution of the nonlinear equation $\mathscr{N}(\bar{\delta}) = 0$ as similar as possible, after numerical calculation, we get the better choice of A and B:

$$A = \lambda - 0.125 \tag{67}$$

$$B = 0.8 \tag{68}$$

The 0th-order deformation equation is constructed as follows:

$$(1-p)\mathscr{L}(\bar{\delta}) + p\mathscr{N}(\bar{\delta}) = 0 \tag{69}$$

Equivalent to:

$$(1-p)(\ddot{\bar{\delta}}+A\bar{\delta}_m\dot{\bar{\delta}}+B\bar{\delta}_m\bar{\delta})+p\left(\ddot{\bar{\delta}}+2\lambda\bar{\delta}\cdot\dot{\bar{\delta}}+\bar{\delta}^2\right)=0 \tag{70}$$

Where, $p\in[0,1]$ is the embedded homotopy parameter, $\dot{\bar{\delta}}$ and $\ddot{\bar{\delta}}$ are the first derivative and the second derivative of $\bar{\delta}$ versus $\bar{t}$, respectively. It can be seen that when p continuously changes from 0 to 1, Eq. (70) continuously changes from the linear equation $\mathscr{L}(\bar{\delta})=0$ to the nonlinear equation $\mathscr{N}(\bar{\delta})=0$ that we need to solve, that is, Eq. (15).

Write the nth-order solution of Eq. (70) into the power series form of p:

$$\bar{\delta}_{n\text{th}}=\sum_{i=0}^{n}\bar{\delta}_i p^i \tag{71}$$

Substitute the series solution(71) into (70) and sort out according to the power of p:

$$\sum_{i=0}^{n}\Delta_i p^i=0 \tag{72}$$

Where Δ_i is expressed as follows:

$$\begin{cases}\Delta_0=\ddot{\bar{\delta}}_0+A\bar{\delta}_m\dot{\bar{\delta}}_0+B\bar{\delta}_m\bar{\delta}_0 i=0\\ \Delta_i=\ddot{\bar{\delta}}_i+A\bar{\delta}_m\dot{\bar{\delta}}_i+B\bar{\delta}_m\bar{\delta}_i-A\bar{\delta}_m\dot{\bar{\delta}}_{i-1}-B\bar{\delta}_m\bar{\delta}_{i-1}+2\lambda\sum_{k=0}^{i-1}\bar{\delta}_k\dot{\bar{\delta}}_{i-1-k}+\sum_{k=0}^{i-1}\bar{\delta}_k\bar{\delta}_{i-1-k} i\geqslant 1\end{cases} \tag{73}$$

Let $p=1$, and the nth-order solution of $\mathscr{N}(\bar{\delta})=0$ is:

$$\bar{\delta}_{n\text{th}}=\sum_{i=0}^{n}\bar{\delta}_i \tag{74}$$

To make Eq. (72) hold when $p=1$, each Δ_n should be equal to 0, so $\bar{\delta}_i$ should satisfy the nth-order linear constraint equation:

$$\begin{cases}\ddot{\bar{\delta}}_0+A\bar{\delta}_m\dot{\bar{\delta}}_0+B\bar{\delta}_m\bar{\delta}_0=0 & i=0\\ \ddot{\bar{\delta}}_i+A\bar{\delta}_m\dot{\bar{\delta}}_i+B\bar{\delta}_m\bar{\delta}_i=A\bar{\delta}_m\dot{\bar{\delta}}_{i-1}+B\bar{\delta}_m\bar{\delta}_{i-1}-2\lambda\sum_{k=0}^{i-1}\bar{\delta}_k\dot{\bar{\delta}}_{i-1-k}-\sum_{k=0}^{i-1}\bar{\delta}_k\bar{\delta}_{i-1-k}\triangleq f_i(\bar{t}) & i\geqslant 1\end{cases} \tag{75}$$

$\bar{\delta}_i$ in Eq. (75) can be solved sequentially from order 0 with the following initial conditions:

$$\begin{cases}\bar{\delta}_0|_{\bar{t}=0}=0,\quad \dot{\bar{\delta}}_0\Big|_{\bar{t}=0}=1 \quad \text{when} \quad i=0\\ \bar{\delta}_i|_{\bar{t}=0}=0,\quad \dot{\bar{\delta}}_i\Big|_{\bar{t}=0}=0 \quad \text{when} \quad i\geqslant 0\end{cases} \tag{76}$$

First, find the 0th-order solution. When $n=0$, it can be obtained from Eq. (74): $\bar{\delta}_{0\text{th}}=\bar{\delta}_0$. The 0th-order linear constraint equation is the damped free vibration equation, and its characteristic equation is $x^2+A\bar{\delta}_m x+B\bar{\delta}_m=0$, and its characteristic root is $x_{1,2}=-0.5A\bar{\delta}_m\pm 0.5\sqrt{4B\bar{\delta}_m-A^2\bar{\delta}_m^2}\sqrt{-1}$. The situation when the recovery rate $e>0$ is our concern. At this time, corresponding to the under damping state, $4B\bar{\delta}_m-A^2\bar{\delta}_m^2>0$ is required. It can be verified that even when this requirement is not met, the analytical solution obtained below is effective through complex operation. At the same time, using the initial conditions (76), we can obtain the 0th-order solution is:

$$\bar{\delta}_{0\text{th}}=\bar{\delta}_0=\frac{1}{\omega}e^{-\beta\bar{t}}\sin(\omega\bar{t}) \tag{77}$$

Where:

$$\beta=\frac{A\bar{\delta}_m}{2} \tag{78}$$

$$\omega=\frac{\sqrt{4B\bar{\delta}_m-A^2\bar{\delta}_m^2}}{2} \tag{79}$$

Then we solve the 1st-order solution. When $n=1$, obtained from Eq. (74):

$$\bar{\delta}_{1\text{st}}=\bar{\delta}_0+\bar{\delta}_1 \tag{80}$$

$\bar{\delta}_0$ is known in Eq.(77), only $\bar{\delta}_1$ needs to be solved. By substituting $i=1$ into Eqs. (75) and (76), we can get the first order linear constraint equation and its initial conditions:

$$\ddot{\bar{\delta}}_1+A\bar{\delta}_m\dot{\bar{\delta}}_1+B\bar{\delta}_m\bar{\delta}_1=A\bar{\delta}_m\dot{\bar{\delta}}_0+B\bar{\delta}_m\bar{\delta}_0-2\lambda\bar{\delta}_0\dot{\bar{\delta}}_0-\bar{\delta}_0\bar{\delta}_0\triangleq f_1(\bar{t}) \tag{81}$$

$$\bar{\delta}_1|_{\bar{t}=0}=\dot{\bar{\delta}}_1\Big|_{\bar{t}=0}=0 \tag{82}$$

Use the constant variation method to solve, let:

$$\bar{\delta}_1=e^{-\beta\bar{t}}[C_{11}(\bar{t})\sin(\omega\bar{t})+C_{12}(\bar{t})\cos(\omega\bar{t})] \tag{83}$$

Substituting it into (81) yields:

$$\begin{cases} C_{11}^{'}(\bar{t})\sin(\omega\bar{t}) + C_{12}^{'}(\bar{t})\cos(\omega\bar{t}) = 0 \\ C_{11}^{'}(\bar{t})\cos(\omega\bar{t}) + C_{12}^{'}(\bar{t})\sin(\omega\bar{t}) = \dfrac{1}{\omega}e^{\beta\bar{t}}f_1(\bar{t}) \end{cases} \tag{84}$$

The solution is:

$$\begin{cases} C_{11}^{'}(\bar{t}) = \dfrac{\cos(\omega\bar{t})}{\omega}e^{\beta\bar{t}}f_1(\bar{t}) \\ C_{12}^{'}(\bar{t}) = -\dfrac{\sin(\omega\bar{t})}{\omega}e^{\beta\bar{t}}f_1(\bar{t}) \end{cases} \tag{85}$$

$C_{11}(0) = C_{12}(0) = 0$ can be obtained from the initial condition (82), so $C_{11}(\bar{t})$ and $C_{12}(\bar{t})$ are expressed in the form of definite integral:

$$\begin{cases} C_{11}(\bar{t}) = \displaystyle\int_0^{\bar{t}} \dfrac{\cos(\omega\bar{t})}{\omega}e^{\beta\bar{t}}f_1(\bar{t})d\bar{t} \\ C_{12}(\bar{t}) = \displaystyle\int_0^{\bar{t}} -\dfrac{\sin(\omega\bar{t})}{\omega}e^{\beta\bar{t}}f_1(\bar{t})d\bar{t} \end{cases} \tag{86}$$

Each item in the integral symbol is the product of the trigonometric function and the exponential function of the natural constant. It is easy to get the analytical expression for their integration. Moreover, the results of $C_{11}(\bar{t})$ and $C_{12}(\bar{t})$ are still composed of the product of the trigonometric function and the exponential function of the natural constant, hence $\bar{\delta}_1$ is obtained.

Similarly, $\bar{\delta}_i$ can be obtained:

$$\bar{\delta}_i = e^{-\beta\bar{t}}[C_{i1}(\bar{t})\sin(\omega\bar{t}) + C_{i2}(\bar{t})\cos(\omega\bar{t})] \tag{87}$$

Where:

$$\begin{cases} C_{i1}(\bar{t}) = \displaystyle\int_0^{\bar{t}} \dfrac{\cos(\omega\bar{t})}{\omega}e^{\beta\bar{t}}f_i(\bar{t})d\bar{t} \\ C_{i2}(\bar{t}) = \displaystyle\int_0^{\bar{t}} -\dfrac{\sin(\omega\bar{t})}{\omega}e^{\beta\bar{t}}f_i(\bar{t})d\bar{t} \end{cases} \tag{88}$$

Finally, the nth-order solution of the nonlinear differential equation is obtained by using Eq. (74).

Why we use HAM? As shown by Fernández, the HAM is merely another presentation of Taylor series for many differential equations (Fernández and Francisco, 2010; Fernández and Francisco, 2020; Fernández, 2020). However, for the present case, the power series expansion method and the small parameter expansion method are not so efficient to solve Eq. (15); the solution converges too slowly to be recognized as an usable solution for the entire history of contact depth, as shown in Fig. A4. The polynomial result with 50th-order obtained by the small parameter expansion method and the polynomial result with 100th-order obtained by the power series expansion method both diverge rapidly near the maximum contact depth. However, HAM shows much better convergence from 0th-order solution.

A4. Force and duration of contact

Fig. A5(a) shows the contact force history when the dissipation factor $\lambda = 0$. The energy dissipation due to the flexural waves of the plate is neglected. Current theory degrades to the Conway impact model and the whole system is conservative. The contact force history is symmetrical. When the dissipation factor $\lambda > 0$, the symmetry of contact force profile is destroyed, as shown in Fig. A5(b), (c) and (d), the stronger the asymmetry as the λ increases. It can also be found that the 1st-order solution is effective in predicting contact force history.

From Eq. (34), the maximum contact force is obtained at the maximum contact depth, and the maximum dimensionless contact force is:

$$\bar{F}_m = \bar{\delta}_m^2 \tag{89}$$

Substituting Eq. (23) into Eq. (89) yields:

$$\bar{F}_m = \left(\lambda + \left(\frac{3}{2}\right)^{-2/3}\right)^{-1} \tag{90}$$

The maximum contact depth at different λ values can be obtained by using the analytical solution and FEM, hence the maximum contact force can also be obtained. As shown in Fig. A6, the Eq. (90) coincides with the 2nd-order solution and is in agreement with the FEM results. The results of the 0th-order solution and the 1st-order solution are also accurate. The results of the 0th-order solution are slightly larger when λ is small, while the results of the 1st-order solution are slightly larger when λ is large. When $\lambda = 0$, the maximum dimensionless contact force reaches the maximum value of 1.310; With the increase of λ, the maximum dimensionless contact force decreases and the rebound velocity decreases. When λ approaches infinity, the maximum contact force tends to zero as indicated by Eq. (90).

Moreover, the dimensionless total contact duration $\bar{t}_t$, dimensionless compression duration $\bar{t}_c$ and dimensionless recovery duration $\bar{t}_r$ can be obtained by analytical solution and plotted on Fig. A7(a), (b) and (c). By fitting the total duration obtained by the numerical method, we get a semi-analytical expression of the total contact duration:

$$\bar{t}_t = 3.210\exp\left(0.476\lambda^{1.182}\right) \tag{91}$$

Material failure is most likely to occur when the contact depth and contact force reach maximum at $\bar{t}_c$. The semi-analytical expression of $\bar{t}_c$ is also given:

$$\bar{t}_c = 1.605\exp\left(-0.158\lambda^{0.697}\right) \tag{92}$$

Eqs. (91) and (92) are plotted in Fig. A7(a) and (b), respectively, and they agree well with the FEM results. With the increase of λ, the total contact duration and recovery duration both increase, while the compression duration decreases, resulting in an increase in the asymmetry of contact history. Let the asymmetry parameter be:

$$\eta = \frac{\bar{t}_r}{\bar{t}_c} \tag{93}$$

As shown in Fig. A7 (d), η increases rapidly from 1 as λ increases.

References

Achenbach, J.D., 1975. Wave Propagation in Elastic Solids. Elsevier.

Argatov, I., 2011. Depth-sensing indentation of a transversely isotropic elastic layer: second-order asymptotic models for canonical indenters. Int. J. Solids Struct. 48 (25–26), 3444–3452.

Argatov, I.I., Jin, X., Keer, L.M., 2021. Depth-sensing spherical indentation of an elastic sphere on an elastic substrate. J. Mech. Phys. Solids 149, 104297.

Boettcher, R., Kunik, M., Eichmann, S., Russell, A., Mueller, P., 2017a. Revisiting energy dissipation due to elastic waves at impact of spheres on large thick plates. Int. J. Impact Eng 104, 45–54.

Boettcher, R., Russell, A., Mueller, P., 2017b. Energy dissipation during impacts of spheres on plates: Investigation of developing elastic flexural waves. Int. J. Solids Struct. 106, 229–239.

Carretero-González, R., Khatri, D., Porter, M.A., Kevrekidis, P., Daraio, C., 2009. Dissipative solitary waves in granular crystals. Phys. Rev. Lett. 102 (2), 024102.

Chiu, C.-C., Liou, Y., 1995. Low-velocity impact damage in brittle coatings. J. Mater. Sci. 30 (4), 1018–1024.

Choi, N.-S., Chang, J.-Y., Kwak, S.-B., Gu, J.-U., 2010. Impact surface fractures of glass-fiber/epoxy lamina-coated glass plates by small steel-ball. Compos. Sci. Technol. 70 (14), 2056–2062.

Conway, H., Engel, P., Lee, H., 1972. Force-time investigations for the elastic impact between a rigid sphere and a thin layer. Int. J. Mech. Sci. 14 (8), 523–529.

Conway, H.D., Lee, H.C., Bayer, R.G., 1970. The impact between a rigid sphere and a thin layer. J. Appl. Mech. 37 (1), 159–162.

Dimitriadis, E.K., Horkay, F., Maresca, J., Kachar, B., Chadwick, R.S., 2002. Determination of elastic moduli of thin layers of soft material using the atomic force microscope. Biophys. J . 82 (5), 2798–2810.

Fernández and Francisco, M., 2020. Comment on 'Analytical approach for solving population balances: a homotopy perturbation method'(2019) J. Phys. A: Math. Theor. 52385201. Journal of Physics A: Mathematical and Theoretical, 53(38): 388001.

Fernández and Francisco, M. On two new applications of the homotopy analysis method and the homotopy perturbation method Physica Scripta 81 3 2010 037002.

M, F. and Fernández, 2020. Comment on: "Neutron star under homotopy perturbation method" Ann. Phys. 409, 167918 Annals of Physics 412 2019 168039.

González, M., Saidman, S., 2011. Electrodeposition of polypyrrole on 316L stainless steel for corrosion prevention. Corros. Sci. 53 (1), 276–282.

Harikumar, R., Devaraju, A., 2020. Exploration of mechanical properties of polyurea coated mild steel plate and aluminium plate sandwich composites. Mater. Today:. Proc. 22, 1144–1148.

Huang, Y., et al., 2006. A model of size effects in nano-indentation. J. Mech. Phys. Solids 54 (8), 1668–1686.

Hunter, S.C., 1957. Energy absorbed by elastic waves during impact. J. Mech. Phys. Solids 5 (3), 162–171.

Hunter, S., 1960. The Hertz problem for a rigid spherical indenter and a viscoelastic half-space. J. Mech. Phys. Solids 8 (4), 219–234.

Jaffar, M., 1988. A numerical solution for axisymmetric contact problems involving rigid indenters on elastic layers. J. Mech. Phys. Solids 36 (4), 401–416.

Job, S., Melo, F., Sokolow, A., Sen, S., 2005. How Hertzian solitary waves interact with boundaries in a 1D granular medium. Phys. Rev. Lett. 94 (17), 178002.

Koller, M., Kolsky, H., 1987. Waves produced by the elastic impact of spheres on thick plates. Int. J. Solids Struct. 23 (10), 1387–1400.

Lan, P., Meyer, J.L., Vaezian, B., Polycarpou, A.A., 2016. Advanced polymeric coatings for tilting pad bearings with application in the oil and gas industry. Wear 354, 10–20.

Li, H., et al., 2022. Optimal design of vibro-impact resistant fiber reinforced composite plates with polyurea coating. Compos. Struct. 292, 115680.

Liu, J., et al., 2018. Puncture mechanics of soft elastomeric membrane with large deformation by rigid cylindrical indenter. J. Mech. Phys. Solids 112, 458–471.

Liu, J., et al., 2022. Indentation of elastomeric membranes by sphere-tipped indenters: Snap-through instability, shrinkage, and puncture. J. Mech. Phys. Solids 167, 104973.

Medick, M.A., 1961. On classical plate theory and wave propagation. J. Appl. Mech. 223–228.

Müller, P., et al., 2016. Contact time at impact of spheres on large thin plates. Adv. Powder Technol. 27 (4), 1233–1243.

Nasrollahi, A., Rizzo, P., 2020. Modeling a new dynamic approach to measure intraocular pressure with solitary waves. J. Mech. Behav. Biomed. Mater. 103, 103534.

Nix, W.D., Gao, H., 1998. Indentation size effects in crystalline materials: a law for strain gradient plasticity. J. Mech. Phys. Solids 46 (3), 411–425.

Peng, B., Feng, X.-Q., Li, Q., 2020. Decohesion of a rigid flat punch from an elastic layer of finite thickness. J. Mech. Phys. Solids 139, 103937.

Peng, Q., Jin, Y., Liu, X., Wei, Y., 2021a. Effect of plasticity on the coefficient of restitution of an elastoplastic sphere impacting an elastic plate. Int. J. Solids Struct. 222, 111036.

Peng, Q., Liu, X., Wei, Y., 2021b. Elastic impact of sphere on large plate. J. Mech. Phys. Solids 156, 104604.

Peng, Q., Liu, X., Shi, X., Wei, Y., 2022. Revisiting the interaction of highly nonlinear solitary wave with wall: From infinite to finite thickness. Int. J. Solids Struct. 241, 111509.

Rahimzadeh, T., Arruda, E.M., Thouless, M., 2015. Design of armor for protection against blast and impact. J. Mech. Phys. Solids 85, 98–111.

Reed, J., 1985. Energy losses due to elastic wave propagation during an elastic impact. J. Phys. D Appl. Phys. 18 (12), 2329.

Russell, A., 2020. On the mechanical properties of coarse particulate products. University of Magdeburg.

Saha, R., Xue, Z., Huang, Y., Nix, W.D., 2001. Indentation of a soft metal film on a hard substrate: strain gradient hardening effects. J. Mech. Phys. Solids 49 (9), 1997–2014.

Shariyat, M., Ghajar, R., Alipour, M., 2012. An analytical solution for a low velocity impact between a rigid sphere and a transversely isotropic strain-hardening plate supported by a rigid substrate. J. Eng. Math. 75 (1), 107–125.

Sneddon, I.N., 1951. Fourier transforms. McGraw-Hill Book Company Inc, New York.

Stergiou, T., Baxevanakis, K.P., Roy, A., Sazhenkov, N.A., Silberschmidt, V.V., 2021. Impact of polyurea-coated metallic targets: Computational framework. Compos. Struct. 113893.

Vergara, L., 2010. Model for dissipative highly nonlinear waves in dry granular systems. Phys. Rev. Lett. 104 (11), 118001.

Wang, H., et al., 2017. Experimental and theoretical analyses of elastic-plastic repeated impacts by considering wave effects. European Journal of Mechanics-A/Solids 65, 212–222.

Xia, Y., Shi, Z., Zhou, Q., Ao, W., 2023. Numerical investigation on polyurea coated aluminum plate subjected to low velocity impact. Int. J. Impact Eng 104516.

Xiao, Y., Tang, Z., Hong, X., 2021. Low velocity impact resistance of ceramic/polyurea composite plates: experimental study. J. Mech. Sci. Technol. 35 (12), 5425–5434.

Zener, C., 1941. The intrinsic inelasticity of large plates. Phys. Rev. 59 (8), 669.